Quaternary Science Reviews 302 (2023) 107718

Contents lists available at ScienceDirect

Quaternary Science Reviews

journal homepage: www.elsevier.com/locate/quascirev

Research Paper

# Paleoglaciology of the central East Antarctic Ice Sheet as revealed by blue-ice sediment

M.R. Kaplan [a, *], K.J. Licht [b], J.L. Lamp [a], G. Winckler [a, c], J.M. Schaefer [a, c], J.A. Graly [d], C.M. Kassab [b], R. Schwartz [a]

[a] Geochemistry, Lamont-Doherty Earth Observatory, Palisades, NY 10964, USA
[b] Department of Earth Sciences, IUPUI, Indianapolis, IN 46202, USA
[c] Department of Earth and Environmental Sciences, Columbia University, New York, NY 10027, USA
[d] Deptartment of Geography and Environmental Science, Northumbria University, Newcastle-Upon-Tyne, NE1 8ST, UK

ARTICLE INFO

*Article history:*
Received 30 March 2022
Received in revised form
10 August 2022
Accepted 11 August 2022
Available online 24 September 2022

Handling Editor: C. O'Cofaigh

*Keywords:*
Cosmogenic dating
Law glacier
Holocene
Antarctica
Paleoclimate
Pleistocene
Deglaciation

ABSTRACT

We present ~100 cosmogenic surface exposure ages, including 75 new analyses, for a blue-ice moraine complex at Mt. Achernar, head of Law Glacier, in the central Transantarctic Mountains. The $^{10}$Be–$^{3}$He–$^{26}$Al ages along with previously-published boron concentrations chronicle past behavior of the East Antarctic Ice Sheet (EAIS) along the edge of the polar plateau since the sediments started to accumulate, around 0.5–1 Ma. Samples analyzed for $^{10}$Be from the Law Glacier surface record <100 years of exposure, indicating they likely have negligible inheritance when first exposed. The Law Glacier surface experienced relatively minor fluctuations in surface elevation throughout MIS 6 and 5, and likely during prior periods, as geomorphic features are intact and exposure ages are coherent on the moraine, ranging from ~210 to ~86 ka; respective means for MIS 5 till in two different areas are 106 ± 9.1 ka [n = 4 ages] and 106 ± 5.1 ka [n = 6]. Although we infer the Law Glacier has been relatively close to its current configuration generally since 0.5–1 Ma, disturbances to Achernar blue-ice moraine architecture seem apparent at times especially prior to the last two glacial cycles. The largest observed disturbance occurred when the nearby Lewis Cliffs Ice Tongue expanded either close to, or earlier than, 500-400 ka. A minimum ice thickness increase of 30 m is associated with the ~20 ka blue-ice ridges, and a lateral moraine indicates the Law Glacier surface was ~40–50 m higher at ~9.2 ± 0.5 ka. Our findings support that lateral accretion over time formed the Mt. Achernar blue-ice moraine sequence, and by implication, other analogue Antarctic deposits. We interpret blue-ice moraines as representing, at times, relatively constant outlet glacier conditions and concur with prior studies that they reflect near-equilibrium forms. Blue-ice sediments are an underutilized and dateable paleoglaciologic and paleoclimate archive in Antarctica, including for former ice surface dynamics and possibly as a repository of old ice during periods such as MIS 5 and prior.



## 1. Introduction

In paleoglaciology, former ice surfaces and their dynamics can be difficult to reconstruct as evidence is not typically left behind. This is especially true for past ice sheet interiors, including for those that still exist in Antarctica. In particular, observations of former ice sheet surfaces are not common prior to the global last glacial maximum (LGM), including in Antarctica. Blue ice ablation zones and their moraines are common throughout the Antarctic continental interior, and provide a unique means to reconstruct the surfaces of former ice sheets, including prior to the LGM (Bintanja, 1999). The primary reason is that their sediment accumulations overlie ice that is adjacent to and linked into active glacier flow (Whillans and Cassidy, 1983; Cassidy et al., 1992; Bintanja, 1999; Sinisalo and Moore, 2010).

Reconstructing past ice surface elevations is important for multiple reasons. First, we can use such evidence to document the relative stability or instability of the interior of the EAIS and other sectors of Antarctica, including during past warm periods. Second, blue-ice sediment and ice arrive from below the surface (Whillans

* Corresponding author.
*E-mail address:* mkaplan@ldeo.columbia.edu (M.R. Kaplan).

https://doi.org/10.1016/j.quascirev.2022.107718
0277-3791/

and Cassidy, 1983; Chinn, 1991, 1994; Cassidy et al., 1992; Corti et al., 2008; Sinisalo and Moore, 2010; Palmer et al., 2012). Hence, their study improves understanding of subglacial, englacial, and supraglacial processes, as well as underlying geology that cannot be observed (Fogwill et al., 2012; Palmer et al., 2012; Ackert et al., 2013; Campbell et al., 2013; Hein et al., 2016; Westoby et al., 2016; Winter et al., 2016; Bader et al., 2017; Graly et al., 2018a,b, 2020). Third, observations of past surfaces and outlet glacier behavior provide test beds for model experiments (Pattyn, 2010; Whitehouse et al., 2012; Golledge et al., 2013; Joy et al., 2014; DeConto and Pollard, 2016), including the sensitivity of different sectors of Antarctica to past warm periods. Last, age information on past surfaces may reveal sites where old ice is preserved (Higgins et al., 2015).

Detailed study of blue-ice sediments is required to understand better these features as important paleoglaciologic and paleoclimate archives. Blue-ice areas typically occur under compressive glaciological regimes where rates of sublimation and wind scouring exceed accumulation. Studies in West Antarctica show that blue-ice regions offer a dateable archive of former ice sheet behavior over the million year timescale (Fogwill et al., 2012; Hein et al., 2016; Woodward et al., 2022). In the Transantarctic Mountains (TAM) blue-ice areas also provide repositories of old ice (e.g., Higgins et al., 2015), because compressive stresses related to flow around the Transantarctic Mountains and sublimation bring subglacial and englacial ice towards the surface from lower, older sections of the ice sheets (Whillans and Cassidy, 1983; Corti et al., 2008).

Here, we provide $^{10}$Be–$^{3}$He–$^{26}$Al cosmogenic surface exposure ages near Mt. Achernar in the central TAM and synthesize all chronologic data with prior efforts in the area (Figs, 1, 2). We use the findings to answer questions concerning the timing, amount, and stability of former ice surface changes at the head of the Law Glacier (Fig. 1) at the edge of the polar plateau, where ice converges into the central TAM. Model output shows that this sector of the EAIS may be relatively insensitive to past climate changes including warm periods (e.g., DeConto and Pollard, 2016). The data allow us to evaluate whether such simulations are consistent with observations, specifically those documenting the magnitude of changes if the central EAIS has been relatively stable.

## 2. Background

### 2.1. Mt. Achernar setting

The Mt. Achernar blue-ice moraine complex begins approximately 20 km downstream of the EAIS plateau. The blue-ice area exists at the head of Law Glacier, which is between the Queen Alexandra and Queen Elizabeth Ranges. Topographic steering into a lee-side embayment (Fig. 1) downstream of Mt. Achernar (2691 m) traps upward flowing ice in a blue-ice area, which subsequently sublimates. Near the active Law Glacier ice/moraine edge (Fig. 3) subsurface-derived debris bands are emerging parallel/subparallel to the margin, and document how en- and subglacial sediment is added to the moraine (Kassab et al., 2020).

The Achernar blue-ice moraine is ~100 km$^2$ and extends >5 km from the active Law Glacier towards the Lewis Cliffs Ice Tongue and other unnamed glaciers that flow more or less northward in the opposite direction (Fig. 1). Located around an elevation of 1700–1900 m, the majority of the moraine complex is dominated by a series of 1–12 m high ridges and troughs that run subparallel to the main flow direction of Law Glacier (Bader et al., 2017). Ridge orientation commonly mimics the shape of the active main trunk of Law Glacier (Fig. 1). Some ridges exhibit laterally continuous visible bands and till of sandstone, dolerite, or mixed lithologies that impart a general color (Fig. 4), which often provided a strategy for sampling. On sunny or relatively warm days with air temperatures still below freezing, we observed surface melting associated with dark-colored debris, especially near the boundary between the moraine and the clean ice of Law Glacier. Although seemingly minor in terms of quantity, we assume such melting may have important geomorphological effects (Graly et al., 2018b) (Fig. 3).

### 2.2. Prior studies at Mt. Achernar

Early studies of the Mt. Achernar area, including around the Lewis Cliffs Ice Tongue and Walcott Névé, were conducted due to the site's usefulness for meteorite collection (e.g., Faure et al., 1992; Cassidy et al., 1992; Hagen, 1995). Scarrow et al. (2014) studied soil chronosequences and patterns of moraine development in this arid setting and inferred that through time material is added so as to thicken progressively the soil from its base, which was documented in later as studies as well (Bader et al., 2017; Graly et al., 2018b). Near the Lewis Cliffs Ice Tongue, Sun et al. (2015) focused on the geochemistry of salts emerging from subglacial water, and argued for a sustained cold polar environment for millions of years.

Bader et al. (2017) presented geomorphic, sedimentologic, and till composition and provenance findings including pebble lithology and detrital zircon geochronology, for the Mt. Achernar moraine complex. They defined 5 zones of the moraine sequence – which we follow in this study – based on color bands and distinct differences in geomorphology; Bader et al. (2017) also found the zones coincided with the relative weathering of sediments and their provenance characteristics. Briefly, Zone 1 tends to be hummocky with pronounced pond-like depressions separated by ridges (Fig. 3). The ridges and depressions exhibit in places a weak alignment that is oriented more or less at an oblique angle to the ice margin (Figs. 2B and 3). Sediments are grey or dark grey. Zone 2 is distinguished by relatively low relief with small ridges far apart (Fig. 4). Zones 3 & 4 contain well-defined continuous parallel/subparallel ridges and troughs (Fig. 4). Zone 4 contains sediments that are pale yellow or light-yellowish brown characteristic of weathering of sandstones, or red varnish that is associated with weathering of the Ferrar Dolerite (Mercer, 1968). Zone 5 sediment contains red varnish and consists of parallel/sub-parallel ridges, and was sourced from the Law Glacier as well as in part from an unnamed northward flowing glacier. In Zone 5, two reported $^{3}$He exposure ages are recalculated from Kaplan et al. (2017), and the boron data are from Graly et al. (2018a).

In the downglacier (northeast) part of the area studied, referred to as the tail, a prominent moraine ridge exhibits characteristics similar to Zone 1 (Bader et al., 2017) (Figs. 2, 5 and 6). Past the moraine ridge (i.e., farther from Law Glacier) exists a snow-covered gap (<20 m wide) and then topographic moraine ridges/troughs. In places, the ridges exhibit a change in orientation so that they are oblique to the innermost moraine ridge (Figs. 1D and 2). On the other side of the snow-covered gap, tail sediments are pale yellow or light yellowish brown or dark red (Ferrar Dolerite) similar to in Zone 4 along the main transect; hence, just based on moraine description we conclude the gap represents a significant temporal discontinuity (Bader et al., 2017; Graly et al., 2018a).

Bader et al. (2017) also described facets and striations on up to 30% of the cobble clasts indicating an active subglacial origin, and concluded that blue-ice sediments contain a valuable record of underlying unexposed bedrock geology that cannot be directly observed. Given there is no exposed bedrock upstream of Mt. Achernar, the moraine sediment is subglacially or englacially derived with mostly local but also some non-local components (Bader et al., 2017), except for meteorites (Cassidy et al., 1992). Over the time interval represented by the moraine complex, Bader et al. (2017) inferred former ice surface changes of <40 m and relatively

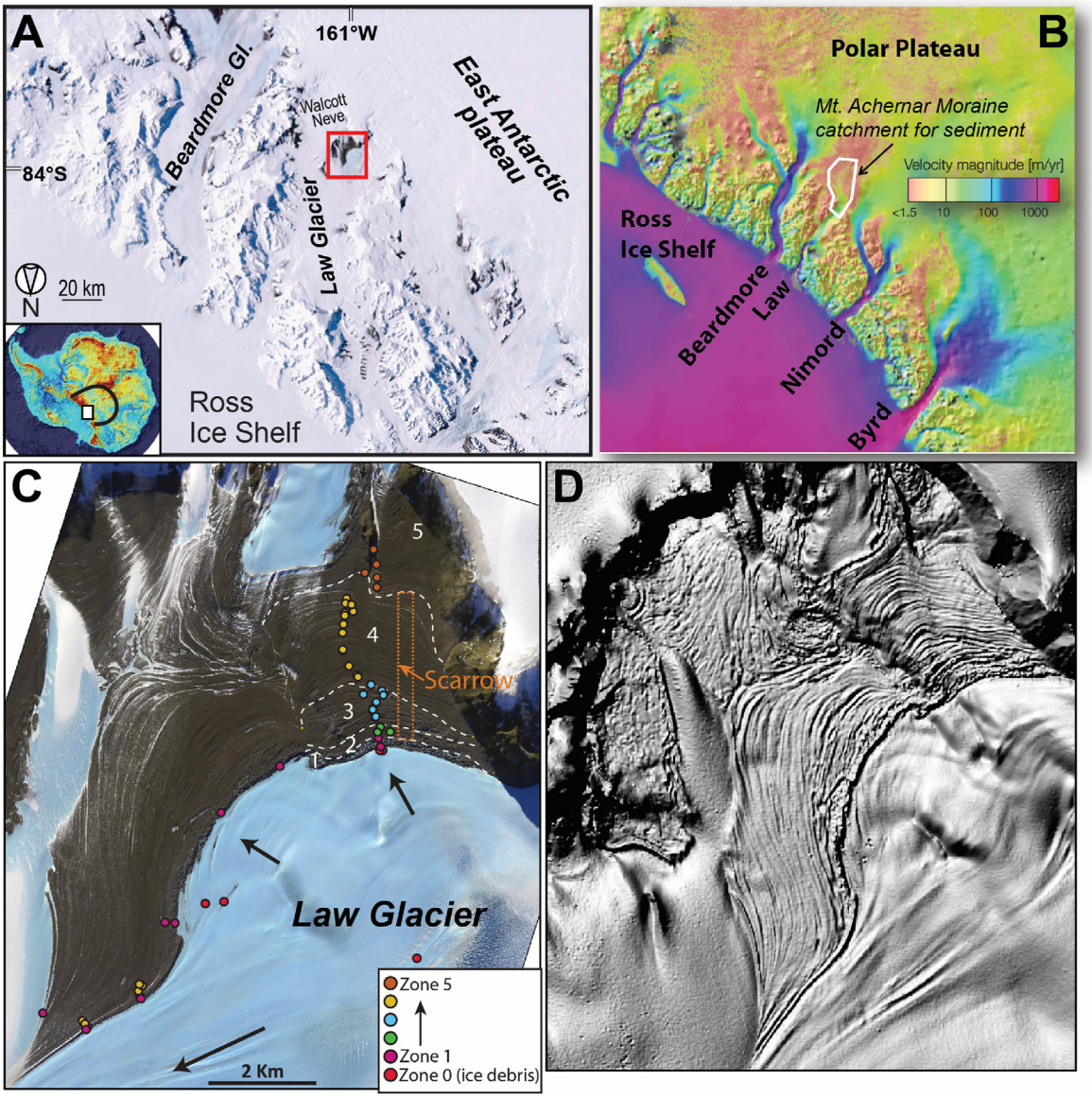


**Fig. 1.** Setting of the Mt. Achernar area. A) Mt. Achernar moraine sits at the head of Law Glacier (within red box) where unconstrained flow off of the East Antarctic plateau becomes constrained through the Transantarctic Mountains. B) Ice surface velocities and sediment catchment area for the Mt. Achernar area (Bader et al., 2017; Graly et al., 2018b). C) The entire moraine complex along with locations of sediment (till) samples for study of provenance changes (Bader et al., 2017) and soil geochemistry (Graly et al., 2018a). Also shown are 5 zones (in white) defined in Bader et al. (2017), the general area of study by Scarrow et al. (2014), and ice flow directions with arrows. Note the ice flow is steered away from the main trunk glacier, where it is then trapped in the embayment (Kassab et al., 2020). D) Image of the Achernar moraine and surrounding area, from Antarctic REMA (Reference Elevation Model of Antarctica) Explorer (Howat et al., 2019). (For interpretation of the references to color in this figure legend, the reader is referred to the Web version of this article.)

stable past ice sheet configurations, in part based on the geomorphology and compositional and provenance studies of glacial till and pebbles.

The first direct chronologies for the Mt. Achernar moraine (Hagen, 1995; Kaplan et al., 2017) established that the site contains sediments exposed at the surface since before the global LGM, during Marine Isotope Stage 2 (MIS 2). Bader et al. (2017) and Kaplan et al. (2017) inferred the East Antarctic polar plateau has been relatively stable for at least 200 kyr. Graly et al. (2018a) analyzed salt concentrations and speciation in the top horizons of Mt. Achernar sediments. They found the concentrations of boron-containing salts are highly correlated to exposure ages of nearby boulders from the same moraine ($R^2 > 0.99$) and inferred that low vapor pressure at cold temperatures and extreme aridity limit mobility of such salt species within the soil column, and major melt could not have occurred during the time the moraine existed. By calibrating boron concentrations in till soils to the first set of cosmogenic nuclide ages available from nearby boulders, Graly et al. (2018a) documented that boron concentration provides a sediment exposure age, which is used in this study.

Most recent studies at Mt. Achernar provided insights into regional subglacial and englacial processes, and general blue-ice moraine sediment formation and soil chemistry. Kassab et al. (2020) integrated ground-penetrating radar (GPR, 100 and 25 MHz) data with GPS measured ice velocity and published surface exposure ages (Kaplan et al., 2017; Graly et al., 2018a). GPR transects (100 and 25 MHz) both perpendicular and parallel to moraine ridges revealed alternating relatively clean ice and horizons where

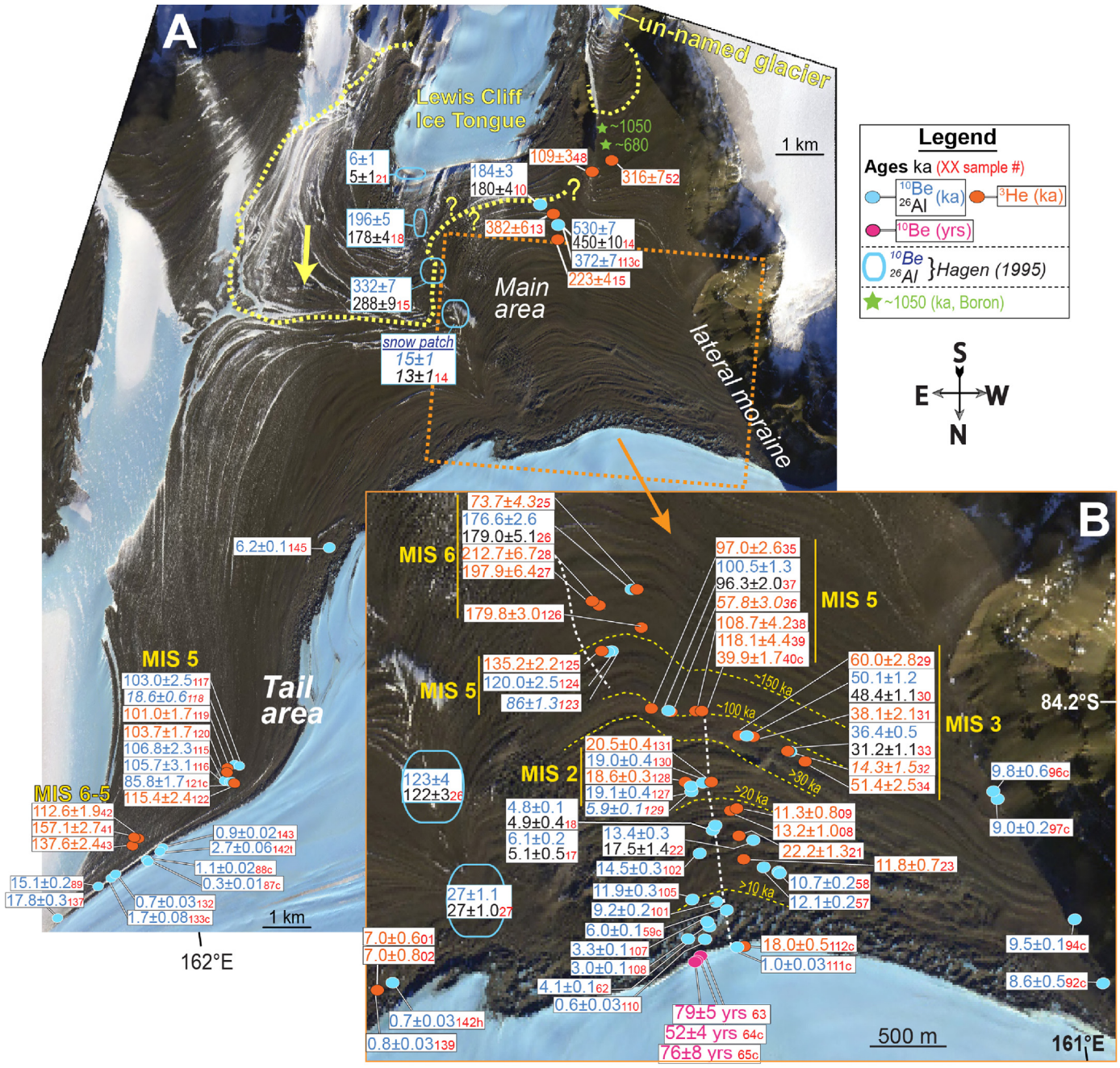


**Fig. 2.** All $^{10}$Be–$^{26}$Al–$^{3}$He ages obtained in the Mt. Achernar area. A) The study area including the tail area (NE sector), which is shown in more detail in Fig. 5. The yellow-dashed line outlines moraine associated with the Lewis Cliffs Ice Tongue, which impinged on and disturbed the Mt. Achernar blue-ice moraine. We show the two oldest boron-exposure ages (Graly et al., 2018a) (Fig. 1C), in the southwestern sector, to the right of Lewis Cliffs Ice Tongue. B) A focus on the main and lateral moraine areas, which are shown in more detail in Fig. 3 and 4. Italicized ages are discussed in text as "possible outliers." All exposure ages are on boulders except those labelled 'c' (cobble-size). All ages in ka, except for three $^{10}$Be ages in pink (years), which are on samples from the Law Glacier margin (see next, Fig. 3 for more detail). Yellow-dashed lines with associated ages mark approximate age boundaries. (For interpretation of the references to color in this figure legend, the reader is referred to the Web version of this article.)

englacial debris bands dip steeply towards the surface. Kassab et al. (2020) suggested sediment generally moves upward associated with debris bands (and along shear planes?), but in certain locations there are more complicated subsurface structures. Kassab et al. (2020) also documented that the entire moraine is underlain by > 150 m glacier ice, with varying amounts of debris in places including in the englacial bands. Along with Graly et al. (2018b), they estimated a maximum elapsed time of ~100–250 kyr from subglacial entrainment to transport and debris reaching the surface. Kassab et al. (2020) proposed a model to explain the formation of blue-ice moraine sequences whereby debris accretes laterally to form new moraine. They also inferred englacial sediments may continue to accumulate at the base of the already-existing moraine, agreeing with the earlier study of Scarrow et al. (2014). Using oxygen isotopes, including those from a shallow core, Graly et al. (2018b) documented that glacier ice flowing upward into the Achernar moraine system was sourced from the EAIS plateau (Fig. 1), and inferred ice and sediment entrainment in an

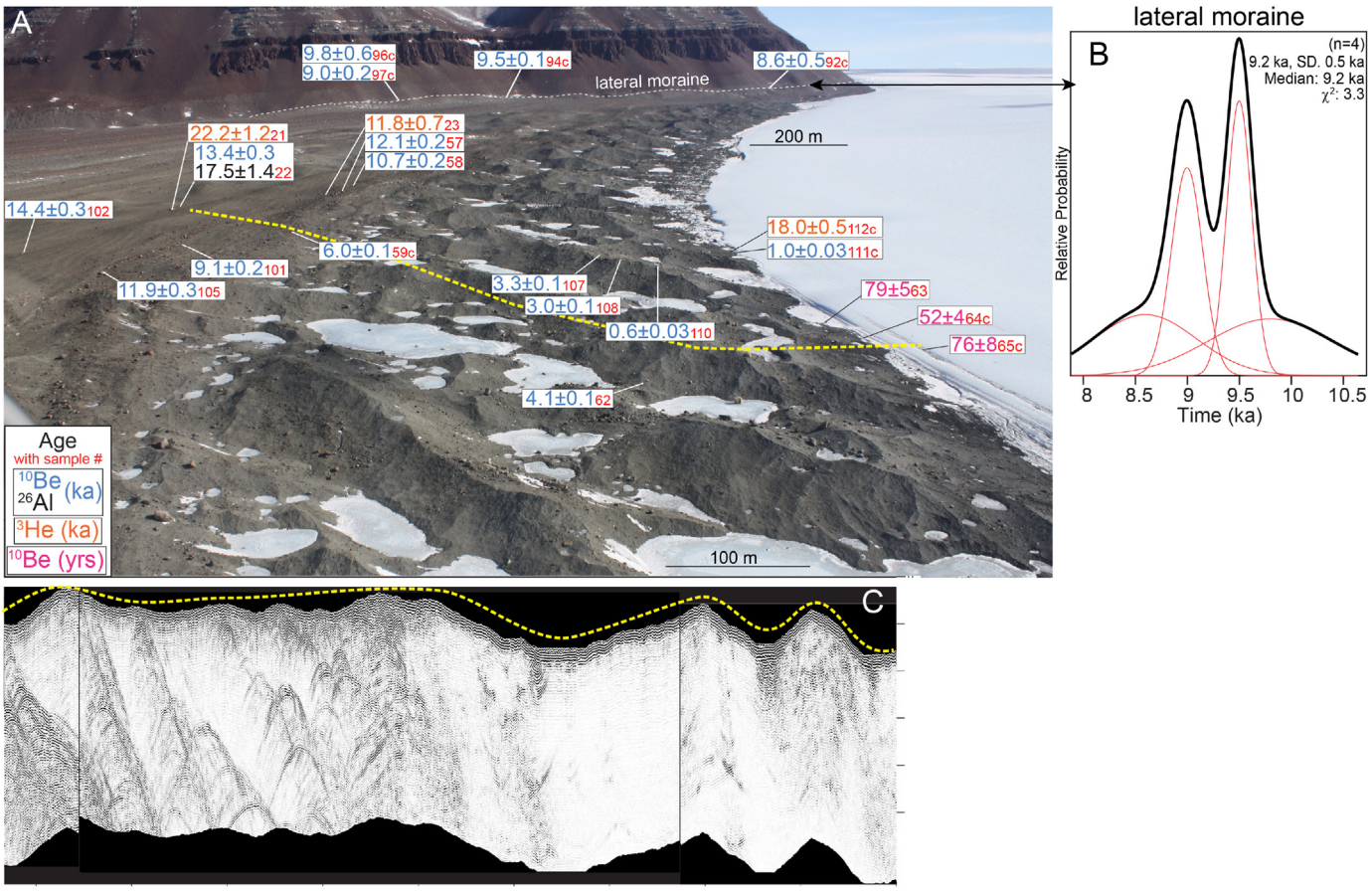


**Fig. 3.** Focus on the best-dated Zones 1 and 2, looking west with the Law Glacier on the right. Headwall of Mt. Achernar shown in background. Four $^{10}$Be ages on samples along the lateral moraine date to 9.2 ± 0.5 ka and record a high surface for ice flowing off the plateau, which is seen in the upper right. GPR radargram profile below the photo is from Kassab et al. (2020), and more or less follows the yellow-dashed line in panel A; dipping stacked and scatterred hyperbolas are inferred to represent planes of debris and cobbles/boulders causing point reflectors, respectively. Fig. 6 provides additional photos of the lateral moraine with samples. (For interpretation of the references to color in this figure legend, the reader is referred to the Web version of this article.)

open system under warm-based basal conditions. Graly et al. (2018b) estimated a minimum age of MIS 6 for the ice underlying and feeding the Achernar blue-ice moraine, and that ice within the current Law Glacier was slightly younger and originated during MIS 5. Last, prior papers argued that the lateral continuity of the ridges and troughs, specifically those with distinct lithologies (Figs. 2 and 4), exposure age progression, and general geochemistry and till provenance signify relative stability of the moraine surface (e.g., Bader et al., 2017; Kaplan et al., 2017; Graly et al., 2018a,b, 2020).

## 3. Methods

We conducted field work at Mt. Achernar during the 2011 and 2015/16 austral summers, either from a nearby base camp ~6–20 km from the moraine sampling sites, or during several 1-day trips by helicopter from the larger CTAM (central TAM) camp. Samples for cosmogenic exposure analyses were collected in three parts of the moraine complex: 1) near and along the main part of the moraine sequence. A main transect, as indicated by the dashed-white line in Fig. 2, is where the majority of samples were collected, and was largely the focus of earlier studies by our group; 2) in the downglacier (southwest) part of the study area, in an area informally referred to as the tail (Figs. 2 and 5); 3) along a lateral moraine that runs along the headwall of Mt. Achernar (Figs. 4 and 6).

We collected quartz-bearing sandstones and pyroxene-bearing dolerites for $^{10}$Be–$^{26}$Al and $^{3}$He, respectively. We sampled mainly boulders (>25 cm high), but also cobbles as noted in the figures and tables. We preferentially selected boulders away from depressions (e.g., polygon boundaries) in areas where periglacial processes were apparent. Samples were taken from the upper 1–3 cm of the boulder, in the most stable-looking, horizontal/flat portion (and if possible as close to the center as possible) of the top surface. Samples were collected with hammer and chisel. A compass and clinometer were used to measure the azimuthal elevations of the surrounding landscape to account for shielding, although it was negligible in almost all cases except for the four lateral moraine samples (~1–1.5% difference in exposure age).

We used a handheld GPS (WGS 84) for all sample latitudes and longitudes. For sample elevations, we used a Trimble GPS system (EGM96), except for 9 sandstones ($^{10}$Be–$^{26}$Al) and 4 dolerites ($^{3}$He) as noted in Table 1. Differential processing used continuous data from a permanent base station set up on a bedrock surface that was 8 km (tail) to 20 km (lateral moraine on Fig. 2) away. For latitude and longitude, we checked all handheld GPS measurements against post-processed differential-based analyses where available, and as expected they are indistinguishable at the scale of all the figures. For elevation, we assume uncertainties are <1 m if differentially based. Comparison of handheld GPS data with differential-based elevations for 104 sites, in which both are available, yields an average offset of +9.1 ± 4.1 m, excluding one sample that was +47.8 m higher. Except for two samples, the handheld GPS

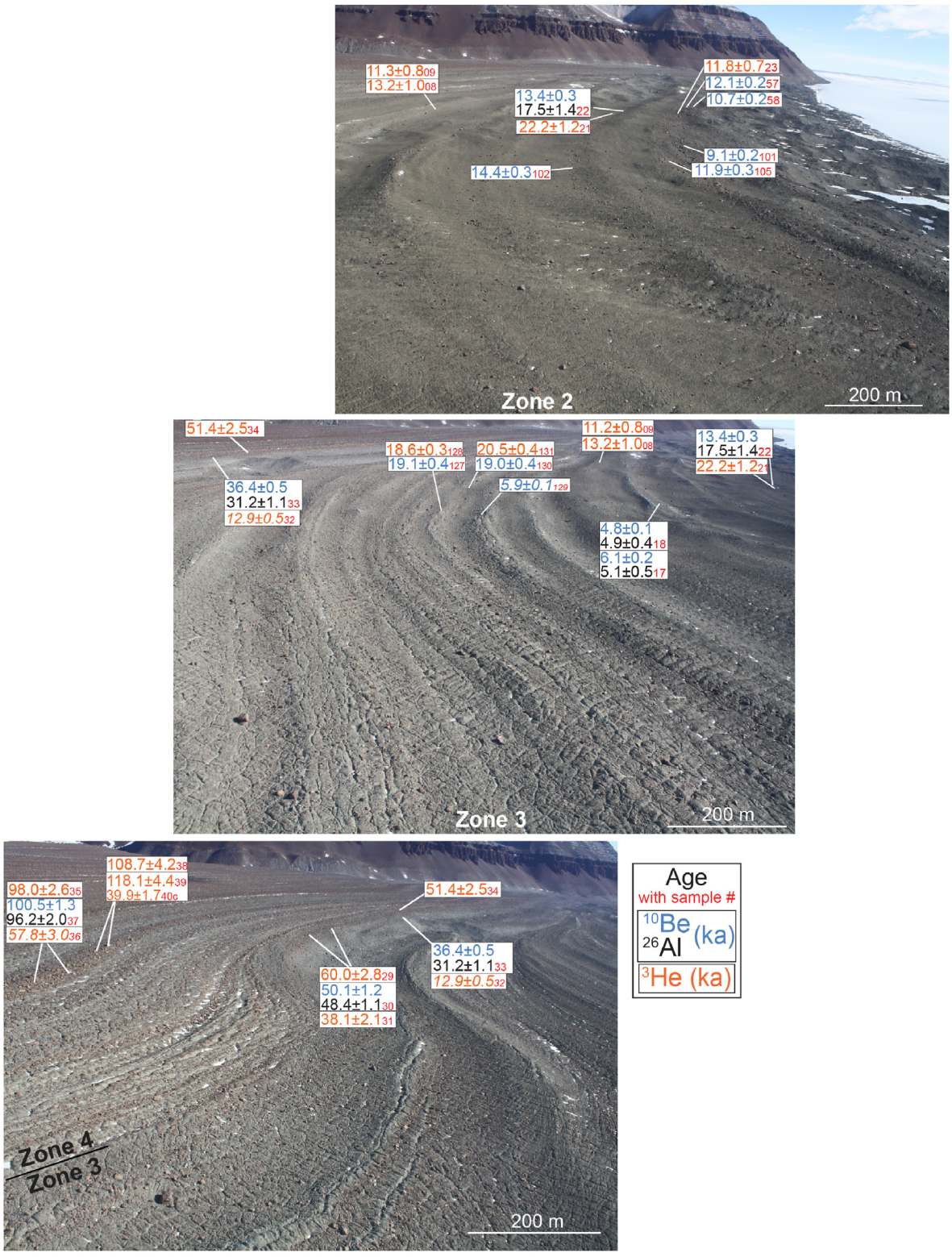


**Fig. 4.** Similar to Fig. 3, with photos focusing on Zones 2 to 4 and cosmogenic exposure ages. Top panel focuses on Zone 2, with the Law Glacier (Fig. 3) on right side. Middle panel focuses on Zones 2 and 3. For moraines dating to MIS 2 time, the average and standard deviation are 19.3 ± 0.8 ka excluding the one outlier of 5.9 ± 0.1. Bottom panel focuses on inner Zone 4 and samples dating to <100 ka. Mt Achernar headwall is in the background. In each subsequent panel, some overlap in exposure ages is shown on right side.

always gave higher elevations. Four samples on one particular moraine ridge were only measured with a handheld GPS, and as noted below in the Results their recorded elevations may be ~10 m too high relative to EGM96 orthometric heights; if correct, this would cause these 4 exposure ages to be <1% too low.

Processing for $^{10}$Be preparation and analyses followed standard procedures at the Lamont Cosmogenic Nuclide Laboratory (Schaefer et al., 2009; Kaplan et al., 2017). A custom-made $^{9}$Be

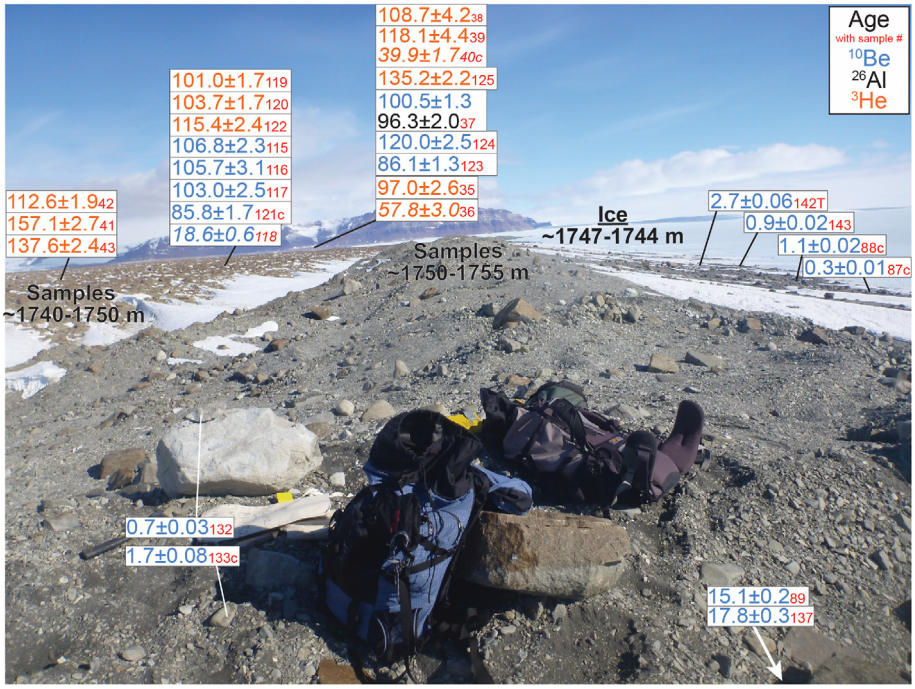


**Fig. 5.** A focus on the tail area, with view looking southwest, towards Mt. Achernar. Law Glacier is on the right. Note relatively oxidized sediments on the left side of the photo, which date to MIS 6 and 5 except for 1 age of ~18.6 ka. Also shown are MIS 5 ages (~135.2–~86.1 ka) from the main moraine area (Fig. 2B), which is in the background (not visible). All ages are on bouldersexcept if labelled "c" (cobble-size sample). Two outliers are italicized. See Fig. 6 for photos that focus on the right side of image; both the ~0.3 and ~0.9 ka ages are slightly closer to the present margin, compared with the ~1.1 and ~2.7 ka ages.

carrier allows measurement of samples with extremely low concentrations, 1000–2000 $^{10}$Be atoms/g (Table 1). Almost all samples were measured at the Center for Accelerator Mass Spectrometry at Lawrence Livermore National Lab, except for nine samples associated with blank BLK2017May10 (Table 1), which were analyzed at PRIME Lab. All $^{26}$Al analyses in this manuscript are from Hagen (1995) or Kaplan et al. (2017), although they were recalculated with up-to-date systematics.

All reported exposure ages were calculated using Version 3 of the online cosmogenic exposure age calculator hosted by the University of Washington (https://hess.ess.washington.edu) (Balco et al., 2008), including ages updated from Kaplan et al. (2017) and Hagen (1995). $^{10}$Be and $^{26}$Al ages are presented based on the production rate calibration dataset from Kaplan et al. (2011) for ~50°S in southern South America, which is the closest geographically to Antarctica. This rate is statistically indistinguishable from the other middle latitude Southern Hemisphere $^{10}$Be production rate calibration, derived in the Southern Alps of New Zealand at ~43°S (Putnam et al., 2010). We present results using three latitude and elevation-dependent production rate scaling methods (St, Lm, LSDn) (Table 3), although for the sake of discussion we show and discuss the time dependent version of Lal (1991)/Stone (2000) (Lm) except where noted.

A recent study by Balter-Kennedy et al. (2020) presented evidence that (at least) at high elevation Antarctic sites and for samples exposed continuously for >$10^6$ years, the production rate calibration based on Borchers et al. (2016) and the LSDn scaling method (Lifton et al., 2014) are perhaps most appropriate for calculating exposure ages. In the Discussion, we also provide ages derived with the rate in Borchers et al. (2016) and LSDn scaling where it may slightly affect our inferences, specifically for the oldest exposure ages. Although we present and discuss ages using Lm (Lal, 1991; Stone, 2000), Table 2 shows differences if LSDn (Lifton et al., 2014) is used instead. For almost all cosmogenic ages, LSDn scaling affords ~10% younger ages than Lm, except for samples exposed for ~1000–2000 years (13–14% younger) and for the last 100 years (0–5% older). If the $^{10}$Be production rate dataset based on Borchers et al. (2016) is used instead of the middle latitude Southern Hemisphere dataset (Kaplan et al., 2011; cf., Putnam et al., 2010), the exposure ages become 5% and 2% lower using the Lm and LSDn scaling methods respectively.

Processing of pyroxene separates and $^3$He analyses followed standard procedures at the Lamont Cosmogenic Nuclide Laboratory (Bromley et al., 2014; Eaves et al., 2015, 2016; Kaplan et al., 2017). Abundance and isotopic analyses are performed with a MAP215-50 noble gas mass spectrometer. Analyses are against either a known volume of a Yellowstone helium standard (MM), or air, as noted in Table 2. As in the case of $^{10}$Be and $^{26}$Al, we used Version 3 of the online calculator at https://hess.ess.washington.edu (Balco et al., 2008) to calculate new, and recalculate previously published (e.g., Kaplan et al., 2017), $^3$He exposure ages. Analogous to $^{10}$Be and $^{26}$Al, we present results from three scaling methods (Table 3), although we show and discuss ages derived with Lm, the time-dependent version of Lal (1991)/Stone (2000), except where noted. Eaves et al. (2015) examined the cosmogenic $^3$He$_{px}$ production rate in the south-west Pacific (39°S) and found it indistinguishable from the default production rate calibration dataset based on Borchers et al. (2016).

$^3$He concentrations and resulting exposure ages presented here are not corrected for noncosmogenic (nucleogenic and inherited mantle-derived) $^3$He in the samples. Unlike in Kaplan et al. (2017), we do not report $^3$He ages with and without subtracting an inferred inherited or nucleogenic fraction. Kaplan et al. (2017) and Balco (2020) recently suggested noncosmogenic concentrations roughly in the mid-$10^6$ atoms/g range consistent with earlier estimates (e.g., Ackert, 2000). As most of the $^3$He exposure ages presented here contain $10^7$-$10^8$ atoms/g (i.e., >10 ka, Tables 2 and 4), the effect is not significant in terms of our findings and conclusions. A future

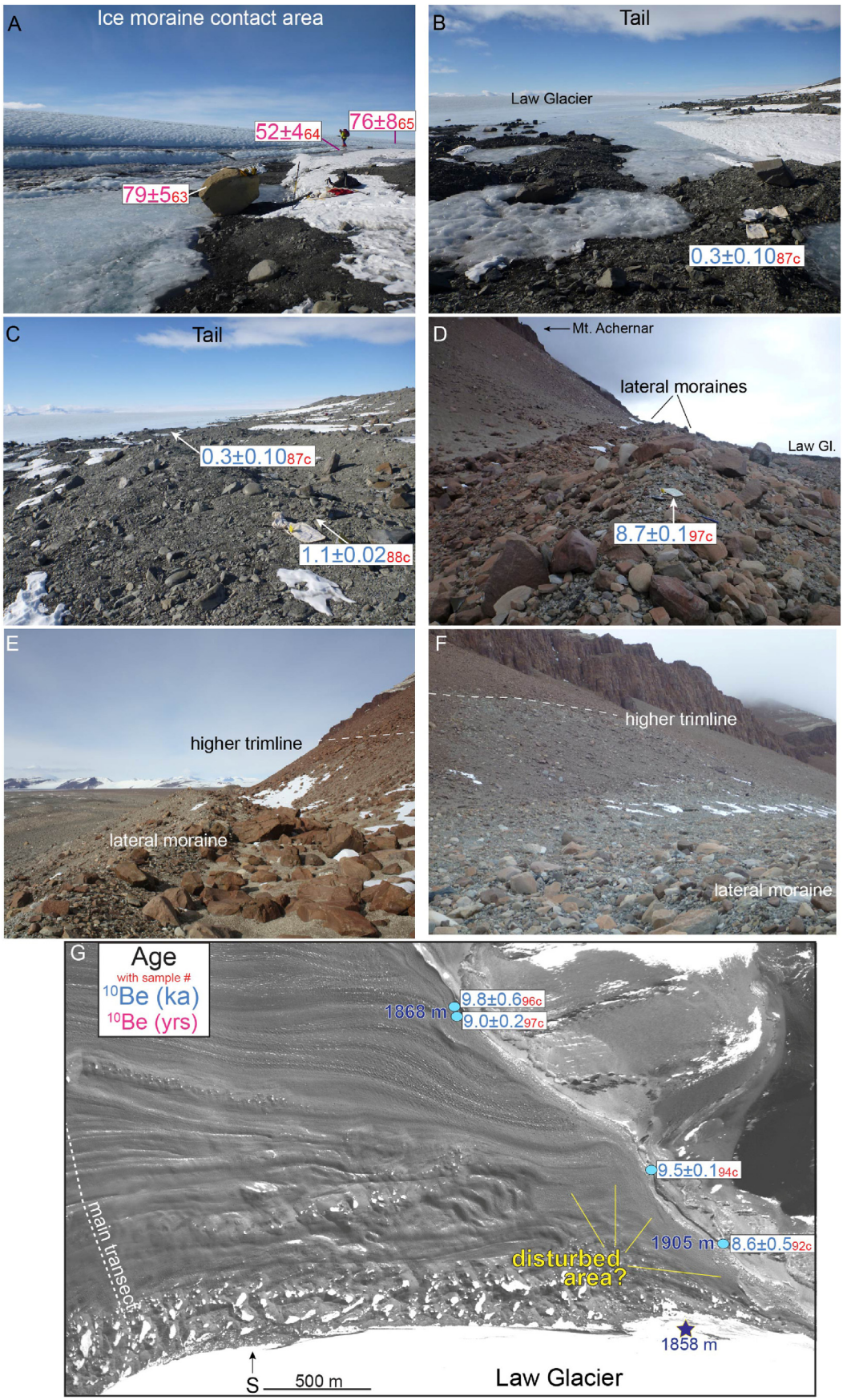
A
Ice moraine contact area
52±4 64
76±8 65
79±5 63
B
Tail
Law Glacier
0.3±0.10 87c
C
Tail
0.3±0.10 87c
1.1±0.02 88c
D
Mt. Achernar
lateral moraines
Law Gl.
8.7±0.1 97c
E
higher trimline
lateral moraine
F
higher trimline
lateral moraine
G
Age
with sample #
10Be (ka)
10Be (yrs)
1868 m
9.8±0.6 96c
9.0±0.2 97c
9.5±0.1 94c
1905 m
8.6±0.5 92c
disturbed area?
1858 m
main transect
S
500 m
Law Glacier

manuscript will discuss such $^{3}$He corrections at Mt. Achernar.

All cosmogenic nuclide exposure ages reported in Tables 3 and 4 assume no erosion. As Antarctica has some of the lowest erosion rates on Earth (Schäfer et al., 1999), for most samples we assume erosion is insignificant. Some of the boulders are still striated (e.g., especially <10 ka). Nonetheless, we point out that if we assume an erosion rate of ~10 cm Ma$^{-1}$, the ~500 ka ages (oldest) increase by ~5%. Also, we do not correct for snow cover on the boulders. We point out that by definition blue-ice areas contain generally little or no snow (Bintanja, 1999). Although some snow may accumulate in small depressions, we avoided sampling in such spots. Hagen (1995) noted that their one young age "outlier" of ~15 ka could be explained by the fact it was collected from a depression with snow (Fig. 2), as mentioned in Kaplan et al. (2017).

## 4. Results

For the ease of presentation, below we describe results separately for three parts of the Mt. Achernar area: the main moraine sequence, the tail area, and the lateral moraine along the headwall of Mt. Achernar (labelled on Fig. 2). In addition, we refer to Zones 1 to 5, as first described in Bader et al. (2017) and elaborated on in Kassab et al. (2020) and reviewed above in Section 2.2. Furthermore, Graly et al. (2018a) sampled several moraines for boron concentrations (Fig. 1c) that were not dated with $^{10}$Be–$^{3}$He–$^{26}$Al. The calibrated boron approach thus adds to the exposure chronology of the entire moraine system (Fig. 7), and ages are mentioned here in Results where pertinent.

### 4.1. Main part of moraine sequence (Figs. 2–4, 6-7)

Most measured samples come from boulders (and 3 cobbles) located close to a transect that was the focus of prior studies, shown by the white-dashed line in Fig. 2. In Zone 1, we analyzed three samples associated with active, relatively clean Law Glacier ice, near the contact with the moraine (Fig. 3). A boulder yields a $^{10}$Be exposure age of 79 ± 5 yrs, and two cobble-sized samples yield ages of 52 ± 4 and 76 ± 8 yrs; thus samples near the Law margin record <100 years of apparent exposure. Two nearby samples around the ice/moraine contact but on the moraine have $^{10}$Be ages ~600–1000 years (MAR-15-110, –111); these results are consistent with two $^{10}$Be ages just to the east (Fig. 2B; MAR-15-139, –142-h), near a small embayment in the moraine, which give essentially identical apparent exposure ages, ~800-700 years. Inward, along Zone 1 sediment (Figs. 3 and 7), exposure ages steadily increase to around 10 ka. Three dolerites yield apparent $^{3}$He ages of ~7 ka and ~14 ka (MAR-11-01,-02, –112c), the first two of which were previously published. As Kaplan et al. (2017) noted, these three apparent exposure ages may record primarily non-cosmogenic $^{3}$He concentrations, with some cosmogenic component given their presence in the middle of Zone 1. Given the large uncertainty for MAR-15-61 (>20%), its age of 2.8 ± 0.7 ka is not used (Table 1).

In Zone 2, exposure ages remain around 14-10 ka, with one discordant $^{26}$Al age slightly older. In Zone 3, ages increase to ~55 ka (Figs. 4 and 7). This includes four coherent ages dating to 19.3 ± 0.8 (excluding one outlier of ~5.9 ka), and a cluster between ~55 and 35 ka (excluding one outlier of ~14.3 ka). We note at least six ridges remain undated in Zone 3.

In Zone 4, we sampled ~5–6 ridges. Exposure ages begin around 100 ka and steadily increase (Figs. 2 and 7). We obtained a large number of ages around 210-177 ka and ~135-86 ka. Four coherent ages date to 106 ± 5.1 ka; in addition, two younger ages on different samples are 57.8 ± 3.0 and 39.9 ± 1.7 ka, respectively, with the lowest age on a cobble-size rock. Slightly farther away from the Law Glacier to the southeast, two ages are 135.2 ± 2.2 and 120.0 ± 2.5 and one nearby younger age is 86.1 ± 1.3. We obtained a cluster of ages from ~213 to 177 ka, along with one younger age of 73.7 ± 4.3 ka. The oldest $^{10}$Be–$^{26}$Al ages towards the back of Zone 4 are ~530-450 ka. The oldest $^{3}$He age is ~380 ka. One cobble-size sample near the ~500 ka boulder dates to ~370 ka. The nearby till boron analyses are consistent with ~500 kyr, or possibly 500-400 kyr, of exposure (Fig. 7; Graly et al., 2018a). Close to the Lewis Cliffs Ice Tongue, exposure ages reverse and become younger. Exposure ages reported in Hagen (1995) are consistent with the new data (Fig. 2). We note that sample elevations for MAR-15-123 to 126 were measured only with a handheld GPS, which tended to be ~10 to 9 m higher than differential-based elevations; if the elevations are too high by ~10 m, the resulting exposure age would be typically ≤1% too low, which is within age uncertainties..

In Zone 5, which is farthest from the Law Glacier (Fig. 1C), two $^{3}$He ages are 109 ± 3 ka (MAR-11-48) and 316 ± 7 ka (MAR-11-52). The ~109 ka boulder is closer to the boundary of sediments associated with the Lewis Cliffs Ice tongue (Fig. 2A), it is greyer in color and located near material with less varnish, and it appears to be surrounded by depressions on the order of a few meters that we assume are caused by periglacial processes. In contrast, the ~316 ka boulder is farther into Zone 5 (Fig. 2A) and surrounded by sediments with extensive red varnish. Closer to the unnamed glacier, slightly farther south, Graly et al. (2018a) obtained the boron exposure ages of ~1 Ma and ~680 ka.

For the entire exposure age distribution in the main sampling area, an exponential relation can describe the increase in $^{10}$Be–$^{3}$He–$^{26}$Al-boron ages with distance from relatively clean Law Glacier ice (Fig. 7), with an $R^2 > 0.7$. For surface sediments exposed <50 kyr, or up to ~2200-2000 m from Law ice, a linear relation also can be used to represent exposure age versus distance, with an $R^2$ of ~0.8 ($^{10}$Be) or ~0.6 ($^{3}$He). That is, a break in slope, or a notable change in the samples' exposure age versus their distance from Law Glacier occurs around 50 ka or at least prior to the last glacial cycle.

### 4.2. Tail area (Fig. 5)

In the downglacier sector of Mt. Achernar, we analyzed samples from recently emerged debris along the edge of the Law Glacier, from the prominent grey-colored, unoxidized moraine positioned east of the ice-contact area, and also from the light-yellowish brown and red till located on the other side (east) of the prominent snow gap (Figs. 2, 5 and 6). Closest to relatively clean Law ice is the youngest exposure age (320 years). A short distance away (~10 m) from Law Glacier and slightly higher (about +4 m), ages increase to ~2700-1100 yrs, similar to those observed in the main area (Figs. 2 and 3). The prominent right lateral ice-cored moraine of grey till is continuous for several kilometers and eventually dissipates downstream. On this moraine, we obtained a relatively

**Fig. 6.** Photos that provide further context of geomorphology and age data. A) Three $^{10}$Be ages near the moraine/Law Glacier boundary. Person for scale. In this panel the three ages are in years, in all other panels they are in ka. B) and C) A focus on the tail area and samples MAR-15-87 (ice margin) and –88 (+4 m). D) The lateral moraine, with two apparent ridges. E) The lateral moraine and trimline, close to (NW of) sample MAR-15-92c (panel G). The tallest boulders are ~1 m in height and we estimate the trimline is about 15–20 m higher. F) The lateral moraine and trimline, by MAR-15-96c (panel G). We estimate the trimline is < 10 m higher. G) The area near the lateral moraine with $^{10}$Be ages (all cobbles). We also show the elevation difference between the Law Glacier (1858 m), lateral moraine (~1905 m), and towards the south (1868 m). Note the area next to the lateral moraine is smoother without distinct ridges, as exists to the left (east) closer to the area of the main transect (white-dashed line, Fig. 2). We infer disturbances within ~500 m of the lateral moraine due to the rise in surface by ~10-9 ka and when the trimline formed.

**Table 1**
Geographical and analytical details for $^{10}$Be and $^{26}$Al samples.

| Sample ID | Latitude (DD) | Longitude (DD) | Elevation (masl) | Sample Thickness (cm) | Shielding correction | Quartz Weight (g) | Carrier (Be) Added (g) | $^{10}$Be/$^{9}$Be ± 1σ | [$^{10}$Be] ± 1σ (atoms x g$^{-1}$) | $^{26}$Al/$^{27}$Al ± 1σ | Total Al | [$^{26}$Al] ±1σ (atoms x g$^{-1}$) | $^{26}$Al/$^{10}$Be |
|---|---|---|---|---|---|---|---|---|---|---|---|---|---|
| MAR-11-22 | −84.18863 | 161.26488 | 1823.14 | 0.61 | 0.999 | 3.0517 | 0.1868 | 8.2943E-14 ± 1.8425E-15 | 338,030 ± 7523 | 2.2501E-13 ± 1.7538E-14 | 1.9849 | 3.2401E+06 ± 2.5254E+05 | 9.6 |
| MAR-11-10 | −84.22163 | 161.35674 | 1847.24 | 1.07 | 1.000 | 10.5039 | 0.1870 | 3.6375E-12 ± 5.2707E-14 | 4,505,087 ± 65,279 | 1.3026E-11 ± 2.3824E-13 | 1.0860 | 3.1280E+07 ± 5.7209E+05 | 6.9 |
| MAR-11-18 | −84.19057 | 161.28288 | 1825.41 | 1.05 | 0.999 | 16.8605 | 0.1874 | 1.4726E-13 ± 2.7890E-15 | 121,259 ± 2298 | 3.1385E-13 ± 2.3831E-14 | 1.9681 | 9.0289E+05 ± 6.8557E+04 | 7.4 |
| MAR-11-26 | −84.2086 | 161.34976 | 1837.80 | 1.67 | 1.000 | 6.8121 | 0.1873 | 3.4409E-12 ± 4.8423E-14 | 4,291,924 ± 60,401 | 7.9704E-12 ± 2.0844E-13 | 1.7343 | 3.0733E+07 ± 8.0373E+05 | 7.2 |
| MAR-11-30 | −84.198 | 161.26189 | 1836.72 | 1.07 | 0.997 | 7.1486 | 0.1881 | 8.5767E-13 ± 2.0059E-14 | 1,258,430 ± 29,433 | 2.2938E-12 ± 5.3104E-14 | 1.4846 | 8.8623E+06 ± 2.0517E+05 | 7.0 |
| MAR-11-37 | −84.2008 | 161.3199 | 1832.74 | 1.36 | 0.999 | 10.0921 | 0.1848 | 2.0383E-12 ± 2.5791E-14 | 2,485,394 ± 31,448 | 4.2631E-12 ± 8.2534E-14 | 1.8284 | 1.7165E+07 ± 3.3232E+05 | 6.9 |
| BLANK_1_ 2012May01 | | | | | | | 0.1871 | 3.4685E-16 ± 1.1828E-16 | | 3.6006E-15 3.6006E-15 | 1.0131 | | |
| BLANK_2_ 2012May01 | | | | | | | 0.1846 | 3.1379E-16 ± 1.0460E-16 | | | 1.6752 | | |
| | | | | | ***average*** = | | 0.1859 | 3.3032E-16 ± 1.1144E-16 | | | | | |
| MAR-11-14a | −84.21938 | 161.33736 | 1845.51 | 2.02 | 1.000 | 4.0553 | 0.1838 | 3.9103E-12 ± 4.2992E-14 | 11,841,897 ± 130,214 | 7.2650E-12 ± 1.3529E-13 | 1.6752 | 6.6932E+07 ± 1.2464E+06 | 5.7 |
| MAR-11-14b | −84.21938 | 161.33736 | 1845.51 | 3.02 | 1.000 | 4.0632 | 0.1852 | 3.8754E-12 ± 4.2663E-14 | 11,798,825 ± 129,907 | 7.3518E-12 ± 1.3708E-13 | 1.6917 | 6.8267E+07 ± 1.2729E+06 | 5.8 |
| MAR-11-17 | −84.19072 | 161.28195 | 1825.76 | 1.10 | 0.999 | 5.0766 | 0.1875 | 6.4713E-14 ± 1.7348E-15 | 154,713 ± 4481 | 1.8906E-13 ± 1.9192E-14 | 1.2010 | 9.5426E+05 ± 9.6869E+04 | 6.2 |
| MAR-11-33 | −84.19702 | 161.25064 | 1836.37 | 1.87 | 0.999 | 8.0920 | 0.1868 | 5.9276E-13 ± 7.6799E-15 | 911,557 ± 11,861 | 1.3267E-12 ± 4.4710E-14 | 1.5731 | 5.7292E+06 ± 1.9308E+05 | 6.3 |
| Blank_2_ 2013Jan24 | | | | | | | 0.1833 | 2.1064E-15 ± 7.0965E-16 | | 6.9381E-15 ± 4.9072E-15 | 1.4472 | | |
| MAR-15-63 | −84.18148 | 161.27971 | 1805.76 | 2.02 | 0.99 | 71.3604 | 0.1881 | 1.2475E-14 ± 6.0648E-16 | 1945 ± 116 | 1.8808E-01 ± 1.2572E+19 | | | |
| MAR-15-89 | −84.1011 | 162.12999 | 1726.54 | 2.90 | 0.99 | 68.2679 | 0.1894 | 1.8575E-12 ± 2.2055E-14 | 344,253 ± 4088 | 1.8942E-01 ± 1.2662E+19 | | | |
| BLK1- 2017Jan20 | | | | | | | 0.1901 | 7.4243E-16 ± 2.6619E-16 | | 1.9015E-01 ± 1.2710E+19 | | | |
| BLK2- 2017Jan20 | | | | | | | 0.1894 | 2.1044E-15 ± 6.0420E-16 | | 1.8942E-01 ± 1.2662E+19 | | | |
| | | | | | ***average*** = | | 0.1898 | 1.4234E-15 ± 4.3520E-16 | | 1.8979E-01 ± 1.2686E+19 | | | |
| MAR-15-57 | −84.1869 | 161.23824 | 1825.56 | 1.30 | 0.99 | 5.0465 | 0.2094 | 1.0989E-13 ± 2.1170E-15 | 302,471 ± 5855 | 2.0939E-01 ± 1.3996E+19 | | | |
| MAR-15-58 | −84.18687 | 161.23439 | 1822.93 | 1.15 | 0.99 | 5.1301 | 0.2102 | 9.8471E-14 ± 1.8819E-15 | 267,457 ± 5142 | 2.1022E-01 ± 1.4052E+19 | | | |
| MAR-15-59 | −84.18513 | 161.26025 | 1821.98 | 4.25 | 0.99 | 9.1888 | 0.2108 | 9.5336E-14 ± 1.7955E-15 | 144,958 ± 2748 | 2.1084E-01 ± 1.4093E+19 | | | |
| Blk1- 2017Mar31 | | | | | | | 0.2108 | 8.5073E-16 ± 2.2658E-16 | | 2.1084E-01 ± 1.4093E+19 | | | |
| Blk2- 2017Mar31 | | | | | | | 0.2111 | 1.0428E-15 ± 2.4995E-16 | | 2.1105E-01 ± 1.4107E+19 | | | |
| MAR-15-62 | −84.18295 | 161.28351 | 1811.08 | 1.16 | 0.99 | 11.8519 | 0.2112 | 8.6337E-14 ± 2.4524E-15 | 101,838 ± 2903 | 2.1116E-01 ± 1.4114E+19 | | | |
| MAR-15-107 | −84.18275 | 161.26979 | 1823.27 | 1.79 | 0.99 | 10.0178 | 0.2111 | 5.8470E-14 ± 1.5704E-15 | 81,180 ± 2199 | 2.1105E-01 ± 1.4107E+19 | | | |
| MAR-15-108 | −84.1826 | 161.27069 | 1823.27 | 1.48 | 0.99 | 10.0021 | 0.2107 | 5.3998E-14 ± 1.5487E-15 | 74,888 ± 2167 | 2.1074E-01 ± 1.4086E+19 | | | |
| *Blk3- 2017Mar31* | | | | | | | *0.2109* | *6.5596E-15 ± 5.1785E-16* | | *2.1095E-01 ± 1.4100E+19* | | | |
| Blk4- 2017Mar31 | | | | | | | 0.2109 | 5.7627E-16 ± 1.4250E-16 | | 2.1095E-01 ± 1.4100E+19 | | | |
| | | | | | ***average*** = | | 0.2109 | 8.2327E-16 ± 2.0634E-16 | | 2.1095E-01 ± 1.4100E+19 | | | |
| MAR-15-101 | −84.18695 | 161.2673 | 1819.72 | 0.88 | 0.99 | 5.0128 | 0.2112 | 8.1879E-14 ± 1.8060E-15 | 229,013 ± 5068 | 2.1119E-01 ± 1.4116E+19 | | | |
| MAR-15-102 | −84.18874 | 161.28691 | 1824.17 | 1.45 | 0.99 | 5.0146 | 0.2106 | 1.2888E-13 ± 2.4900E-15 | 360,163 ± 6971 | 2.1057E-01 ± 1.4075E+19 | | | |
| MAR-15-105 | −84.18724 | 161.27559 | 1819.72 | 1.14 | 0.99 | 5.0264 | 0.2116 | 1.0568E-13 ± 2.4496E-15 | 295,833 ± 6869 | 2.1161E-01 ± 1.4144E+19 | | | |
| MAR-15-110 | −84.18232 | 161.27232 | 1823.27 | 1.56 | 0.99 | 10.264 | 0.2117 | 1.1291E-14 ± 5.7741E-16 | 14,802 ± 781 | 2.1171E-01 ± 1.4151E+19 | | | |
| Blk- 2017Apr24 | | | | | | | 0.2115 | 5.5490E-16 ± 1.4507E-16 | | 2.1150E-01 ± 1.4137E+19 | | | |
| MAR-15-123 | −84.2057 | 161.34746 | 1843 | 1.93 | 0.99 | 5.0634 | 0.2110 | 7.6295E-13 ± 1.1594E-14 | 2,123,403 ± 32,269 | 2.1098E-01 ± 1.4103E+19 | | | |
| MAR-15-124 | −84.20555 | 161.3488 | 1848 | 0.99 | 0.99 | 5.0628 | 0.2113 | 1.0646E-12 ± 2.1445E-14 | 2,968,196 ± 59,794 | 2.1129E-01 ± 1.4123E+19 | | | |
| MAR-15-127 | −84.19295 | 161.28496 | 1826.45 | 0.82 | 0.99 | 5.0203 | 0.2118 | 1.6935E-13 ± 3.2120E-15 | 476,029 ± 9038 | 2.1181E-01 ± 1.4158E+19 | | | |
| MAR-15-129 | −84.19279 | 161.28449 | 1826.45 | 0.51 | 0.99 | 5.1102 | 0.2116 | 5.4337E-14 ± 1.2848E-15 | 148,861 ± 3542 | 2.1161E-01 ± 1.4144E+19 | | | |
| MAR-15-130 | −84.19304 | 161.27354 | 1831.73 | 0.97 | 0.99 | 5.2448 | 0.2115 | 1.7745E-13 ± 3.2912E-15 | 476,819 ± 8852 | 2.1150E-01 ± 1.4137E+19 | | | |

| | | | | | | | | | | | | | |
|---|---|---|---|---|---|---|---|---|---|---|---|---|---|
| MAR-15-61* | −84.18515 | 161.2618 | 1821.98 | 3.55 | 0.99 | 2.2905 | 0.2108 | 1.1178E-14 | ± 2.6466E-15 | 67,678 | ± 16,096 | 2.1075E-01 | ± 1.4087E+19 |
| MAR-15-92* | −84.1783 | 160.98804 | 1904.60 | 4.00 | 0.96 | 2.6515 | 0.2113 | 4.0871E-14 | ± 2.2903E-15 | 216,753 | ± 12,219 | 2.1127E-01 | ± 1.4122E+19 |
| MAR-15-96* | −84.19298 | 161.07387 | 1867.90 | 3.58 | 0.97 | 3.8038 | 0.2109 | 6.5878E-14 | ± 4.0279E-15 | 243,455 | ± 14,914 | 2.1086E-01 | ± 1.4094E+19 |
| MAR-15-113* | −84.21936 | 161.33713 | 1845.51 | 2.03 | 0.99 | 2.4022 | 0.2110 | 1.4587E-12 | ± 2.4562E-14 | 8,561,925 | ± 144,173 | 2.1096E-01 | ± 1.4101E+19 |
| MAR-15-115* | −84.11847 | 161.90501 | 1744.06 | 1.38 | 0.99 | 5.1354 | 0.2109 | 8.9057E-13 | ± 1.8826E-14 | 2,443,724 | ± 51,663 | 2.1086E-01 | ± 1.4094E+19 |
| MAR-15-116* | −84.11846 | 161.90353 | 1744.06 | 0.97 | 0.99 | 5.1346 | 0.2108 | 8.8475E-13 | ± 2.5301E-14 | 2,426,941 | ± 69,401 | 2.1075E-01 | ± 1.4087E+19 |
| MAR-15-117* | −84.11996 | 161.88979 | 1740.26 | 1.37 | 0.99 | 5.0444 | 0.2101 | 8.4521E-13 | ± 1.9706E-14 | 2,352,964 | ± 54,862 | 2.1013E-01 | ± 1.4046E+19 |
| MAR-15-118* | −84.12008 | 161.89259 | 1740.26 | 2.2 | 0.99 | 5.5238 | 0.2104 | 1.6919E-13 | ± 5.6893E-15 | 430,398 | ± 14,487 | 2.1044E-01 | ± 1.4067E+19 |
| BLK-2017May10 | | | | | | | 0.2111 | 1.7418E-16 | ± 2.5100E-16 | | | 2.1107E-01 | ± 1.4108E+19 |
| MAR-15-121* | −84.11846 | 161.90353 | 1744.06 | 4.58 | 0.99 | 5.0141 | 0.2105 | 6.8561E-13 | ± 1.2952E-14 | 1,923,867 | ± 36,351 | 2.1055E-01 | ± 1.4074E+19 |
| MAR-15-64 | −84.18138 | 161.28145 | 1807.76 | 5.17 | 1.00 | 60.2190 | 0.1881 | 6.6579E-15 | ± 4.5087E-16 | 1244 | ± 85 | 1.8806E-01 | ± 1.2570E+19 |
| MAR-15-65 | −84.14503 | 161.65594 | 1807.76 | 5.03 | 1.00 | 60.3486 | 0.1889 | 9.5706E-15 | ± 1.0482E-15 | 1857 | ± 204 | 1.8889E-01 | ± 1.2626E+19 |
| MAR-15-111 | −84.18176 | 161.26093 | 1822 | 5.42 | 1.00 | 59.0633 | 0.1894 | 1.1843E-13 | ± 2.7978E-15 | 25,238 | ± 596 | 1.8941E-01 | ± 1.2660E+19 |
| Blk1-2018Apr12 | | | | | | | 0.1882 | 6.9705E-16 | ± 4.8794E-17 | | | 1.8816E-01 | ± 1.2577E+19 |
| MAR-15-142t | −84.10804 | 162.02833 | 1735.46 | 1.2 | 1.00 | 25.1410 | 0.1884 | 1.2708E-13 | ± 2.9053E-15 | 63,450 | ± 1452 | 1.8840E-01 | ± 1.2593E+19 |
| MAR-15-143 | −84.1079 | 162.03623 | 1735.53 | 2.17 | 1.00 | 25.0331 | 0.1888 | 4.0044E-14 | ± 9.7898E-16 | 19,986 | ± 493 | 1.8881E-01 | ± 1.2621E+19 |
| MAR-15-139 | −84.17844 | 161.54603 | 1765.28 | 2.23 | 1.00 | 15.0371 | 0.1886 | 2.2616E-14 | ± 7.7663E-16 | 18,623 | ± 649 | 1.8861E-01 | ± 1.2607E+19 |
| MAR-15-142h | −84.17929 | 161.53086 | 1762.27 | 1.47 | 1.00 | 15.0697 | 0.1888 | 2.0394E-14 | ± 8.0085E-16 | 16,743 | ± 666 | 1.8881E-01 | ± 1.2621E+19 |
| MAR-15-145 | −84.17109 | 161.65658 | 1753.73 | 1.11 | 1.00 | 15.3124 | 0.1886 | 1.8045E-13 | ± 3.3488E-15 | 148,239 | ± 2753 | 1.8861E-01 | ± 1.2607E+19 |
| Blk1-2018May02 | | | | | | | 0.1886 | 4.5315E-16 | ± 1.4450E-16 | | | 1.8861E-01 | ± 1.2607E+19 |
| MAR-15-132 | −84.10163 | 162.12943 | 1734.24 | 1.91 | 1.00 | 15.6711 | 0.1886 | 2.1908E-14 | ± 9.8354E-16 | 17,301 | ± 784 | 1.8861E-01 | ± 1.2607E+19 |
| MAR-15-133 | −84.1016 | 162.12968 | 1733.24 | 2.39 | 1.00 | 4.0390 | 0.1886 | 1.2773E-14 | ± 5.6459E-16 | 38,610 | ± 1752 | 1.8861E-01 | ± 1.2607E+19 |
| MAR-15-137 | −84.09444 | 162.22047 | 1736 | 2.41 | 1.00 | 25.0135 | 0.1876 | 8.2752E-13 | ± 1.3800E-14 | 414,581 | ± 6914 | 1.8757E-01 | ± 1.2538E+19 |
| MAR-15-94 | −84.18259 | 161.01146 | 1894.53 | 4.22 | 0.96 | 25.2107 | 0.1889 | 4.7329E-13 | ± 5.9397E-15 | 236,863 | ± 2973 | 1.8892E-01 | ± 1.2628E+19 |
| MAR-15-97 | −84.19283 | 161.07315 | 1867.90 | 3.45 | 0.97 | 19.7066 | 0.1887 | 3.4883E-13 | ± 5.9739E-15 | 223,022 | ± 3820 | 1.8871E-01 | ± 1.2614E+19 |
| Blk2-2018May02 | | | | | | | 0.1879 | 3.5369E-16 | ± 1.1799E-16 | | | 1.8788E-01 | ± 1.2558E+19 |
| | | | | | ***average*** = | | | | 1.3124E-16 | | | | |
| MAR-15-76 | −84.14011 | 161.69324 | 1743.05 | 5.13 | 1.00 | 68.8982 | 0.1858 | 7.0104E-15 | ± 3.9843E-16 | 1094 | ± 71 | 1.8582E-01 | ± 1.2420E+19 |
| MAR-15-87 | −84.10684 | 162.04926 | 1731.42 | 5.00 | 1.00 | 71.2908 | 0.1858 | 4.2733E-14 | ± 1.3147E-15 | 7280 | ± 227 | 1.8582E-01 | ± 1.2420E+19 |
| MAR-15-88 | −84.14143 | 161.69112 | 1760 | 4.29 | 1.00 | 70.6214 | 0.1858 | 1.4030E-13 | ± 2.5992E-15 | 24,507 | ± 456 | 1.8582E-01 | ± 1.2420E+19 |
| BLK1-2019Jan31 | | | | | | | 0.1856 | 1.1055E-15 | ± 2.1689E-16 | | | 1.8562E-01 | ± 1.2406E+19 |
| BLK2-2019Jan31 | | | | | | | 0.1853 | 7.8632E-16 | ± 1.7585E-16 | | | 1.8531E-01 | ± 1.2385E+19 |
| | | | | | ***average*** = | | | | 1.9637E-16 | | | | |

Notes: The first two sets of samples (n=10) above the horizontal black line are from Kaplan et al. (2017). Samples with asterisk − associated with blank BLK2017May10 − were analyzed at PRIME Lab, all others were analyzed at CAMS-LLNL. Given large uncertainty for MAR-15-61 (>20%), it is not used. Sample elevations to a whole number were measured with a handheld GPS, otherwise by differential GPS (Trimble). AMS standard used for normalization is 2.85x10-12=07KNSTD3110. Shown are 1σ analytical AMS uncertainties. Column of 9Be added is adjusted for carrier (Be) concentration. Tables also are provided as Supplementary Material.

**Table 2**
Geographical and analytical details for $^{3}$He data.

| Sample ID | Latitude (DD) | Longitude (DD) | Elevation (masl) | Sample Thickness (cm) | Shielding correction | Pyroxene Mass (g) | $^{3}He/^{4}He \pm 1\sigma$ | $[^{3}He] \pm 1\sigma$ (atoms/g) | standard |
|---|---|---|---|---|---|---|---|---|---|
| MAR-11-08 | −84.1910 | 161.2749 | 1829.79 | 1.07 | 0.999 | 0.0719 | 7.4858E+05 ± 8.690E-08 | 9.215E+06 ± 7.486E+05 | MM |
| MAR-11-08 | | | | | | 0.0312 | 8.7819E+05 ± 1.136E-07 | 1.073E+07 ± 8.782E+05 | MM |
| **MAR-11−08 avg** | | | | | | | | 9.973E+06 ± 8.160E+05 | |
| MAR-11-23 | −84.1870 | 161.2414 | 1825.85 | 1.35 | 0.999 | 0.0460 | 1.0899E-07 ± 8.539E-09 | 8.317E+06 ± 5.385E+05 | MM |
| MAR-11-23 | | | | | | 0.0371 | 1.3302E-07 ± 9.684E-09 | 9.397E+06 ± 6.839E+05 | MM |
| **MAR-11−23 avg** | | | | | | | | 8.857E+06 ± 6.155E+05 | |
| MAR-11-52 | −84.2286 | 161.2652 | 1830.53 | 1.09 | 0.999 | 0.0516 | 5.5264E+06 ± 9.438E-06 | 2.380E+08 ± 5.526E+06 | MM |
| MAR-11-48Green | −84.2268 | 161.2755 | 1840.52 | 1.13 | 0.999 | 0.0254 | 2.2413E+06 ± 2.363E-06 | 8.237E+07 ± 2.241E+06 | MM |
| MAR-11-48Red | −84.2268 | 161.2755 | 1840.52 | 1.13 | 0.999 | 0.0263 | 2.2742E+06 ± 3.169E-07 | 8.281E+07 ± 2.274E+06 | MM |
| MAR-11-21AL | −84.1887 | 161.2672 | 1823.14 | 1.09 | 0.999 | 0.0285 | 9.4099E+05 ± 3.169E-07 | 1.769E+07 ± 9.410E+05 | MM |
| MAR-11-21CM | −84.1887 | 161.2672 | 1823.14 | 1.09 | 0.999 | 0.0333 | 8.1605E+05 ± 2.744E-07 | 1.557E+07 ± 8.161E+05 | MM |
| MAR-11-35 | −84.2011 | 161.3220 | 1827.24 | 1.31 | 0.999 | 0.0315 | 1.9503E+06 ± 1.271E-06 | 7.354E+07 ± 1.950E+06 | MM |
| MAR-11-01 | −84.1790 | 161.5365 | 1765.28 | 1.29 | 0.999 | 0.0290 | 4.4749E+05 ± 6.990E-08 | 5.029E+06 ± 4.475E+05 | MM |
| MAR-11-02 | −84.1791 | 161.5366 | 1765.28 | 0.57 | 0.999 | 0.0227 | 5.5215E+05 ± 1.040E-07 | 5.076E+06 ± 5.522E+05 | MM |
| MAR-11-09 | −84.1911 | 161.2725 | 1829.28 | 1.00 | 0.999 | 0.0262 | 5.9883E+05 ± 1.093E-07 | 8.530E+06 ± 5.988E+05 | MM |
| MAR-15-112 | −84.1414 | 161.6911 | 1822 | 3.87 | 0.998 | 0.1250 | 4.1334E-08 ± 1.328E-09 | 1.296E+07 ± 4.063E+05 | Air |
| MAR-15-112 | | | | | | 0.1226 | 4.2506E-08 ± 1.125E-09 | 1.333E+07 ± 3.457E+05 | Air |
| **MAR-15−112_avg** | | | | | | | | 1.315E+07 ± 3.772E+05 | |
| MAR_15_120 | −84.1190 | 161.8995 | 1744.06 | 1.68 | 0.990 | 0.2001 | 4.6848E-06 ± 7.864E-08 | 7.219E+07 ± 1.187E+06 | MM |
| MAR_11_41 | −84.1087 | 162.0593 | 1737.80 | 0.94 | 0.990 | 0.2002 | 6.0928E-07 ± 9.308E-09 | 1.096E+08 ± 1.444E+06 | Air |
| MAR_11_42 | −84.1087 | 162.0578 | 1737.80 | 1.10 | 0.990 | 0.2002 | 2.1186E-07 ± 3.354E-09 | 7.842E+07 ± 1.081E+06 | Air |
| MAR_15_126 | −84.2060 | 161.3452 | 1847 | 1.00 | 0.990 | 0.1993 | 9.8634E-07 ± 1.485E-08 | 1.360E+08 ± 1.761E+06 | Air |
| MAR_15_119 | −84.1198 | 161.8960 | 1740.26 | 1.06 | 0.990 | 0.5028 | 1.1002E-06 ± 1.638E-08 | 7.050E+07 ± 9.003E+05 | Air |
| MAR_15_125_2 | −84.2056 | 161.3483 | 1860 | 2.30 | 0.990 | 0.5008 | 3.1158E-06 ± 4.583E-08 | 1.021E+08 ± 1.281E+06 | Air |
| MAR_15_128_2 | −84.1930 | 161.2859 | 1826.45 | 2.16 | 0.990 | 0.5033 | 2.9126E-07 ± 4.954E-09 | 1.374E+07 ± 2.090E+05 | Air |
| MAR_15_131_2 | −84.1930 | 161.2720 | 1831.73 | 0.99 | 0.990 | 0.4975 | 3.4440E-07 ± 5.719E-09 | 1.533E+07 ± 2.264E+05 | Air |
| MAR_11_13 | −84.2209 | 161.3382 | 1847.94 | 1.09 | 0.990 | 0.2018 | 1.0618E-06 ± 1.556E-08 | 2.889E+08 ± 3.610E+06 | Air |
| MAR_11_15 | −84.2190 | 161.3443 | 1846.23 | 2.15 | 0.990 | 0.2000 | 7.3744E-07 ± 1.103E-08 | 1.673E+08 ± 2.146E+06 | Air |
| MAR_11_43 | −84.1082 | 162.0607 | 1744.17 | 1.07 | 0.990 | 0.2016 | 1.0482E-06 ± 1.611E-08 | 9.634E+07 ± 1.283E+06 | Air |
| MAR_15_122_2 | −84.1185 | 161.9035 | 1744.06 | 3.75 | 0.990 | 0.0731 | 1.3895E-07 ± 2.485E-09 | 7.891E+07 ± 1.271E+06 | Air |
| MAR-11-25 | −84.2087 | 161.3480 | 1837.80 | 1.74 | 0.999 | 0.0111 | 2.2807E-07 ± 1.097E-08 | 5.633E+07 ± 2.425E+06 | MM |
| MAR-11-25b | −84.2087 | 161.3480 | 1837.80 | 1.74 | 0.999 | 0.0193 | 2.3889E-07 ± 2.213E-08 | 5.503E+07 ± 3.936E+06 | MM |
| MAR-11-25b | | | | | | 0.0106 | 2.2388E-07 ± 1.097E-08 | 5.444E+07 ± 2.399E+06 | MM |
| **MAR-11−25b avg** | | | | | | | | 5.473E+07 ± 3.260E+06 | |
| MAR-11-27 | −84.2085 | 161.3655 | 1836.56 | 1.09 | 0.999 | 0.0106 | 8.9096E-07 ± 3.425E-08 | 1.498E+08 ± 4.803E+06 | MM |
| MAR-11-28 | −84.2082 | 161.3619 | 1836.77 | 2.17 | 0.999 | 0.0000 | 5.9706E-07 ± 1.2397E-08 | 1.675E+08 ± 3.455E+06 | Air |
| MAR-11-29 | −84.1980 | 161.2660 | 1835.95 | 1.58 | 0.999 | 0.0247 | 2.9678E-07 ± 1.787E-08 | 4.544E+07 ± 2.217E+06 | MM |
| MAR-11-29 | | | | | | | 3.1097E-07 ± 1.570E-08 | 4.498E+07 ± 2.062E+06 | MM |
| **MAR-11−29 avg** | | | | | | | | 4.521E+07 ± 2.141E+06 | MM |
| MAR-11-31 | −84.1977 | 161.2584 | 1837.49 | 1.11 | 0.999 | 0.0257 | 2.7176E-07 ± 1.701E-08 | 2.463E+07 ± 1.503E+06 | MM |
| MAR-11-31 | | | | | | | 2.2397E-07 ± 1.445E-08 | 3.307E+07 ± 1.702E+06 | MM |
| **MAR-11−31 avg** | | | | | | | | 2.885E+07 ± 1.605E+06 | |
| MAR-11-32 | −84.1970 | 161.2508 | 1836.37 | 1.90 | 0.999 | 0.1144 | 3.8387E-08 ± 1.267E+07 | 1.267E+07 ± 5.055E+05 | Air |
| MAR-11-34 | −84.1971 | 161.2372 | 1836.37 | 1.29 | 0.999 | 0.0117 | 1.7393E-07 ± 9.307E-09 | 3.884E+07 ± 1.908E+06 | MM |
| MAR-11-36 | −84.2008 | 161.3194 | 1832.74 | 0.83 | 0.999 | 0.0181 | 3.7043E-07 ± 2.329E-08 | 4.271E+07 ± 2.227E+06 | MM |
| MAR-11-36 | | | | | | | 3.8036E-07 ± 2.073E-08 | 4.473E+07 ± 2.255E+06 | MM |
| **MAR-11−36 avg** | | | | | | | | 4.372E+07 ± 2.241E+06 | |
| MAR-11-38 | −84.2006 | 161.3078 | 1826.12 | 0.84 | 0.999 | 0.0925 | 2.3212E-07 ± 5.2394E-09 | 9.406E+07 ± 2.112E+06 | Air |
| MAR-11-39 | −84.2006 | 161.3019 | 1827.10 | 0.97 | 0.999 | 0.1158 | 3.7897E-07 ± 0.000E+00 | 1.021E+08 ± 2.255E+06 | Air |
| MAR-11-40 | −84.2006 | 161.3019 | 1827.10 | 2.32 | 0.999 | 0.0254 | 5.8912E-07 ± 2.757E-08 | 2.965E+07 ± 1.244E+06 | MM |

Notes: The samples (n=11) above the horizontal black line are from Kaplan et al. (2017). Sample elevations to a whole number were measured with a handheld GPS, otherwise by differential GPS (Trimble).

**Table 3**
$^{10}$Be,$^{26}$Al ages from Mt. Achernar.

| Sample name | $^{10}$Be Age ± 1σ | | | | $^{10}$Be Age ± 1σ | | | | $^{10}$Be Age ± 1σ | | | | $^{26}$Al Age ± 1σ | | | |
|---|---|---|---|---|---|---|---|---|---|---|---|---|---|---|---|---|
| | St (yrs) | | int. err | ext. err | Lm (yrs) | | int. err | ext. err | LSDn (yrs) | | int. err | ext. err | Lm (yrs) | | int. err | ext. err |
| MAR-11-22 | 13,800 | ± | 310 | 560 | 13,400 | ± | 300 | 540 | 12,100 | ± | 270 | 480 | 17,500 | ± | 1380 | 2160 |
| MAR-11-10 | 189,400 | ± | 2880 | 7300 | 183,500 | ± | 2790 | 6980 | 165,500 | ± | 2500 | 6130 | 180,200 | ± | 3610 | 18,880 |
| MAR-11-18 | 5000 | ± | 90 | 190 | 4800 | ± | 90 | 180 | 4300 | ± | 80 | 160 | 4900 | ± | 370 | 590 |
| MAR-11-26 | 182,300 | ± | 2690 | 6980 | 176,600 | ± | 2600 | 6670 | 159,400 | ± | 2340 | 5870 | 179,000 | ± | 5120 | 19,100 |
| MAR-11-30 | 51,700 | ± | 1220 | 2150 | 50,100 | ± | 1190 | 2070 | 45,300 | ± | 1070 | 1830 | 48,400 | ± | 1150 | 4800 |
| MAR-11-37 | 103,700 | ± | 1350 | 3840 | 100,500 | ± | 1300 | 3670 | 90,900 | ± | 1180 | 3240 | 96,200 | ± | 1950 | 9690 |
| MAR-11-14a | 547,900 | ± | 6930 | 22,390 | 529,300 | ± | 6660 | 21,240 | 473,400 | ± | 5870 | 18,300 | 439,000 | ± | 10,220 | 52,600 |
| MAR-11-14b | 550,700 | ± | 6980 | 22,530 | 532,100 | ± | 6710 | 21,360 | 475,800 | ± | 5910 | 18,410 | 454,600 | ± | 10,690 | 54,930 |
| MAR-11-17 | 6300 | ± | 180 | 280 | 6100 | ± | 180 | 270 | 5600 | ± | 160 | 240 | 5100 | ± | 520 | 710 |
| MAR-11-33 | 37,500 | ± | 490 | 1370 | 36,400 | ± | 480 | 1310 | 32,900 | ± | 430 | 1160 | 31,200 | ± | 1070 | 3160 |
| MAR-15-63 | 82 | ± | 5 | 6 | 79 | ± | 5 | 5 | 81 | ± | 5 | 6 | | | | |
| MAR-15-89 | 15,500 | ± | 190 | 560 | 15,100 | ± | 180 | 540 | 13,700 | ± | 160 | 470 | | | | |
| MAR-15-57 | 12,500 | ± | 240 | 490 | 12,100 | ± | 240 | 470 | 10,900 | ± | 210 | 410 | | | | |
| MAR-15-58 | 11,100 | ± | 210 | 430 | 10,700 | ± | 210 | 410 | 9600 | ± | 190 | 360 | | | | |
| MAR-15-59 | 6100 | ± | 120 | 240 | 6000 | ± | 110 | 230 | 5400 | ± | 100 | 200 | | | | |
| MAR-15-62 | 4200 | ± | 120 | 190 | 4100 | ± | 120 | 180 | 3700 | ± | 110 | 160 | | | | |
| MAR-15-107 | 3400 | ± | 90 | 150 | 3300 | ± | 90 | 140 | 2900 | ± | 80 | 120 | | | | |
| MAR-15-108 | 3100 | ± | 90 | 140 | 3000 | ± | 90 | 130 | 2700 | ± | 80 | 120 | | | | |
| MAR-15-101 | 9500 | ± | 210 | 380 | 9200 | ± | 200 | 370 | 8200 | ± | 180 | 320 | | | | |
| MAR-15-102 | 14,900 | ± | 290 | 580 | 14,500 | ± | 280 | 560 | 13,100 | ± | 250 | 500 | | | | |
| MAR-15-105 | 12,300 | ± | 290 | 510 | 11,900 | ± | 280 | 490 | 10,700 | ± | 250 | 430 | | | | |
| MAR-15-110 | 610 | ± | 32 | 38 | 600 | ± | 31 | 37 | 520 | ± | 27 | 32 | | | | |
| MAR-15-123 | 88,800 | ± | 1380 | 3360 | 86,100 | ± | 1340 | 3220 | 77,900 | ± | 1210 | 2850 | | | | |
| MAR-15-124 | 123,800 | ± | 2570 | 5020 | 120,000 | ± | 2490 | 4810 | 108,400 | ± | 2240 | 4260 | | | | |
| MAR-15-127 | 19,600 | ± | 380 | 770 | 19,100 | ± | 360 | 730 | 17,200 | ± | 330 | 650 | | | | |
| MAR-15-129 | 6100 | ± | 150 | 250 | 5900 | ± | 140 | 240 | 5400 | ± | 130 | 220 | | | | |
| MAR-15-130 | 19,600 | ± | 370 | 760 | 19,000 | ± | 360 | 730 | 17,200 | ± | 320 | 650 | | | | |
| MAR-15-61 | 2900 | ± | 680 | 690 | 2800 | ± | 660 | 670 | 2400 | ± | 580 | 590 | | | | |
| MAR-15-92 | 8900 | ± | 500 | 590 | 8600 | ± | 490 | 570 | 7700 | ± | 440 | 500 | | | | |
| MAR-15-96 | 10,100 | ± | 620 | 710 | 9800 | ± | 600 | 690 | 8800 | ± | 540 | 610 | | | | |
| MAR-15-113 | 384,600 | ± | 7140 | 16,010 | 372,100 | ± | 6890 | 15,250 | 334,200 | ± | 6120 | 13,300 | | | | |
| MAR-15-115 | 110,100 | ± | 2390 | 4510 | 106,800 | ± | 2320 | 4320 | 97,000 | ± | 2100 | 3850 | | | | |
| MAR-15-116 | 109,000 | ± | 3200 | 4960 | 105,700 | ± | 3100 | 4760 | 96,000 | ± | 2810 | 4250 | | | | |
| MAR-15-117 | 106,200 | ± | 2540 | 4480 | 103,000 | ± | 2470 | 4300 | 93,600 | ± | 2230 | 3830 | | | | |
| MAR-15-118 | 19,100 | ± | 650 | 920 | 18,600 | ± | 630 | 880 | 16,900 | ± | 570 | 790 | | | | |
| MAR-15-121 | 88,500 | ± | 1710 | 3500 | 85,800 | ± | 1660 | 3360 | 78,000 | ± | 1500 | 2990 | | | | |
| MAR-15-64 | 53 | ± | 4 | 4 | 52 | ± | 4 | 4 | 54 | ± | 4 | 4 | | | | |
| MAR-15-65 | 79 | ± | 9 | 9 | 76 | ± | 8 | 9 | 78 | ± | 9 | 9 | | | | |
| MAR-15-111 | 1070 | ± | 25 | 44 | 1040 | ± | 25 | 42 | 890 | ± | 21 | 36 | | | | |
| MAR-15-142t | 2800 | ± | 60 | 110 | 2700 | ± | 60 | 110 | 2400 | ± | 50 | 90 | | | | |
| MAR-15-143 | 880 | ± | 22 | 37 | 850 | ± | 21 | 35 | 730 | ± | 18 | 30 | | | | |
| MAR-15-139 | 800 | ± | 28 | 39 | 780 | ± | 27 | 38 | 670 | ± | 23 | 32 | | | | |
| MAR-15-142h | 720 | ± | 29 | 37 | 700 | ± | 28 | 36 | 600 | ± | 24 | 31 | | | | |
| MAR-15-145 | 6400 | ± | 120 | 250 | 6200 | ± | 120 | 240 | 5600 | ± | 110 | 210 | | | | |
| MAR-15-132 | 760 | ± | 34 | 43 | 740 | ± | 33 | 42 | 640 | ± | 29 | 36 | | | | |
| MAR-15-133 | 1700 | ± | 80 | 100 | 1700 | ± | 80 | 90 | 1400 | ± | 70 | 80 | | | | |
| MAR-15-137 | 18,400 | ± | 310 | 700 | 17,800 | ± | 300 | 670 | 16,200 | ± | 270 | 590 | | | | |
| MAR-15-94 | 9800 | ± | 120 | 350 | 9500 | ± | 120 | 340 | 8500 | ± | 110 | 300 | | | | |
| MAR-15-97 | 9300 | ± | 160 | 350 | 9000 | ± | 150 | 340 | 8000 | ± | 140 | 300 | | | | |
| MAR-15-87 | 330 | ± | 10 | 15 | 320 | ± | 10 | 15 | 290 | ± | 9 | 13 | | | | |
| MAR-15-88 | 1100 | ± | 20 | 40 | 1100 | ± | 20 | 40 | 900 | ± | 20 | 40 | | | | |

Notes: External errors (ext) provided in addition to internal (analytical) errors. The samples above the horizontal black line are from Kaplan et al. (2017), and ages are recalculated as discussed in Methods.

wide age distribution from ~1 ka to 18 ka. A boulder and cobble (MAR-15-132, −133) provided ages of ~740 years and ~1.7 ka, respectively. Close to these two ages of <2 ka, and still on the grey unoxidized moraine, is a boulder age of 15.1 ± 0.2 ka. At the end of the tail is another boulder age of 17.8 ± 0.3 ka. The two boulder ages ~15–18 ka are located in the last ~1200 m before the tail debris dissipates, and they do not appear to have a relation with distance from the Law ice edge; the ~15.1 ka boulder is located slightly closer to the Law margin compared with the 1.7 ka sample.

East of the grey moraine by ~50 m, samples were collected from the light-yellowish brown and red oxidized till. Here moraine ridges are oblique to the grey moraine and six $^{10}$Be–$^{3}$He dates offer a coherent age cluster of 103.1 ± 8.9 ka, or 105.9 ± 5.1 ka excluding an age of 85.8 ± 1.7 ka, and an obvious outlier of ~18.6 ka (Fig. 5). A second set of three $^{3}$He ages slightly farther to the southeast (MAR-11-41 to 43) range from 160 to110 ka. There is a difference of about 60–80 kyr – close to a full glacial cycle – between the light-yellowish brown/red oxidized and the unoxidized moraine areas. The unoxided and oxided sediments are at similar elevations, with the latter (i.e., lateral moraine) being slightly higher by ~5–10 m. The light-yellowish brown and red oxidized sector is about the same elevation as the modern ice surface, ~1750-1740 m (Fig. 5).

### 4.3. Lateral moraine along headwall of Mt. Achernar

Four cobble-sized samples were $^{10}$Be dated along a lateral moraine that runs along the west-side headwall that bounds the Achernar moraine complex (Figs. 2 and 3). The ages form a

**Table 4**
$^{3}$He ages from Mt. Achernar.

| Sample name | $^{3}$He Age ± 1σ | | | | $^{3}$He Age ± 1σ | | | | $^{3}$He Age ± 1σ | | | |
|---|---|---|---|---|---|---|---|---|---|---|---|---|
| | St (yrs) | | int. err | ext. err | Lm (yrs) | | int. err | ext. err | LSD (yrs) | | int. err | ext. err |
| MAR-11-08 | 13,200 | ± | 1010 | 1770 | 13,240 | ± | 1010 | 1770 | 12,090 | ± | 920 | 1620 |
| MAR-11-23 | 11,800 | ± | 720 | 1490 | 11,820 | ± | 720 | 1490 | 10,770 | ± | 660 | 1360 |
| MAR-11-52 | 315,900 | ± | 7340 | 35,510 | 315,880 | ± | 7330 | 35,510 | 290,120 | ± | 6740 | 32,620 |
| MAR-11-48Green | 108,500 | ± | 2950 | 12,300 | 108,550 | ± | 2950 | 12,300 | 99,580 | ± | 2710 | 11,280 |
| MAR-11-48Red | 109,100 | ± | 3000 | 12,370 | 109,120 | ± | 3000 | 12,370 | 100,100 | ± | 2750 | 11,350 |
| MAR-11-21AL | 23,600 | ± | 1260 | 2880 | 23,600 | ± | 1260 | 2880 | 21,620 | ± | 1150 | 2640 |
| MAR-11-21CM | 20,800 | ± | 1090 | 2530 | 20,780 | ± | 1090 | 2530 | 19,030 | ± | 1000 | 2320 |
| MAR-11-35 | 98,000 | ± | 2600 | 11,090 | 98,030 | ± | 2600 | 11,090 | 90,010 | ± | 2390 | 10,190 |
| MAR-11-01 | 7000 | ± | 630 | 990 | 7020 | ± | 630 | 990 | 6460 | ± | 570 | 910 |
| MAR-11-02 | 7000 | ± | 770 | 1090 | 7040 | ± | 770 | 1090 | 6480 | ± | 700 | 1000 |
| MAR-11-09 | 11,300 | ± | 800 | 1480 | 11,320 | ± | 800 | 1480 | 10,300 | ± | 720 | 1340 |
| MAR-15-112_avg | 18,000 | ± | 520 | 2050 | 18,000 | ± | 520 | 2050 | 16,470 | ± | 470 | 1870 |
| MAR_15_120 | 103,700 | ± | 1710 | 11,530 | 103,700 | ± | 1710 | 11,530 | 95,780 | ± | 1580 | 10,650 |
| MAR_11_41 | 157,100 | ± | 2670 | 17,490 | 157,110 | ± | 2670 | 17,490 | 145,210 | ± | 2470 | 16,160 |
| MAR_11_42 | 112,600 | ± | 1930 | 12,540 | 112,610 | ± | 1930 | 12,540 | 104,060 | ± | 1790 | 11,590 |
| MAR_15_126 | 179,800 | ± | 3030 | 20,010 | 179,810 | ± | 3030 | 20,010 | 164,910 | ± | 2780 | 18,350 |
| MAR_15_119 | 101,000 | ± | 1670 | 11,240 | 101,010 | ± | 1670 | 11,240 | 93,310 | ± | 1540 | 10,380 |
| MAR_15_125_2 | 135,200 | ± | 2230 | 15,040 | 135,210 | ± | 2230 | 15,040 | 123,870 | ± | 2050 | 13,780 |
| MAR_15_128_2 | 18,600 | ± | 370 | 2080 | 18,630 | ± | 370 | 2080 | 17,040 | ± | 340 | 1910 |
| MAR_15_131_2 | 20,500 | ± | 400 | 2290 | 20,490 | ± | 400 | 2290 | 18,750 | ± | 360 | 2090 |
| MAR_11_13 | 382,000 | ± | 6040 | 42,450 | 381,980 | ± | 6040 | 42,450 | 350,400 | ± | 5540 | 38,940 |
| MAR_11_15 | 223,500 | ± | 3660 | 24,860 | 223,530 | ± | 3660 | 24,860 | 205,050 | ± | 3360 | 22,800 |
| MAR_11_43 | 137,600 | ± | 2410 | 15,330 | 137,640 | ± | 2410 | 15,330 | 127,150 | ± | 2220 | 14,160 |
| MAR_15_122_2 | 115,400 | ± | 2380 | 12,920 | 115,400 | ± | 2380 | 12,920 | 106,600 | ± | 2200 | 11,930 |
| MAR-11-25 | 74,800 | ± | 3220 | 8830 | 74,780 | ± | 3220 | 8830 | 68,590 | ± | 2950 | 8100 |
| MAR-11-25b | 72,700 | ± | 4330 | 9090 | 72,660 | ± | 4330 | 9090 | 66,640 | ± | 3970 | 8340 |
| MAR-11-27 | 197,900 | ± | 6350 | 22,680 | 197,930 | ± | 6350 | 22,680 | 181,680 | ± | 5830 | 20,820 |
| MAR-11-28 | 212,700 | ± | 6680 | 24,340 | 212,730 | ± | 6680 | 24,340 | 195,270 | ± | 6130 | 22,340 |
| MAR-11-29 | 60,000 | ± | 2840 | 7190 | 60,020 | ± | 2840 | 7190 | 55,040 | ± | 2610 | 6590 |
| MAR-11-31 | 38,100 | ± | 2120 | 4700 | 38,100 | ± | 2120 | 4700 | 34,900 | ± | 1940 | 4300 |
| MAR-11-32 | 14,300 | ± | 1530 | 2190 | 14,270 | ± | 1530 | 2190 | 13,020 | ± | 1400 | 2000 |
| MAR-11-34 | 51,400 | ± | 2530 | 6190 | 51,420 | ± | 2530 | 6190 | 47,140 | ± | 2320 | 5680 |
| MAR-11-36 | 57,800 | ± | 2960 | 7010 | 57,800 | ± | 2960 | 7010 | 53,010 | ± | 2720 | 6430 |
| MAR-11-38 | 108,700 | ± | 4220 | 12,680 | 108,660 | ± | 4220 | 12,680 | 99,780 | ± | 3880 | 11,640 |
| MAR-11-39 | 118,100 | ± | 4360 | 13,700 | 118,080 | ± | 4360 | 13,700 | 108,430 | ± | 4000 | 12,580 |
| MAR-11-40 | 39,900 | ± | 1670 | 4690 | 39,870 | ± | 1670 | 4690 | 36,560 | ± | 1530 | 4310 |

Notes: External errors (ext) provided in addition to internal (analytical) errors. The samples above the horizontal black line are from Kaplan et al. (2017), and ages are recalculated as discussed in Methods.

relatively coherent distribution with a mean age of 9.2 ± 0.5 ka. The moraine is approximately 40–50 m above the current clean ice margin (Fig. 6D–F), and is oriented more or less in the direction of flow into the lee side embayment and towards the Mt. Achernar moraine (Kassab et al., 2020), and oblique to the flow of the trunk of Law Glacier (Fig. 1). The moraine slopes about 20 m/km southeastward towards the middle of the moraine complex and appears to end in inner Zone 4, just past the 100 ka ridges of the main area. There is a trimline that is higher than the lateral moraine, by <20 m and <10 m, close to Law Glacier and adjacent to inner Zone 4, respectively. This trimline remains undated and is discussed further in Section 5.3.

### 4.4. Boulders vs cobbles

We sampled cobble-sized sediments to compare their exposure ages with those of boulders. By the ice/moraine contact, one boulder and two cobbles have similar apparent exposure ages (~80-50 yrs). In the back of Zone 4, one cobble-size sample (MAR-15-113c) was analyzed near the ~500 ka boulder and is notably younger (370 ± 7 ka). For comparison, the nearby boron concentration is consistent with 500–400 kyr of exposure (Fig. 7; Graly et al., 2018a). In the tail area, the cobble-sized sample (MAR-15-88) has a $^{10}$Be result (~1.1 ka) consistent with other nearby boulders and cobbles; in addition, it is slightly farther (~10–20 m) away from the sample exposed for less time, ~320 yrs, and current clean ice boundary (Figs. 5 and 6).

### 4.5. $^{26}$Al and $^{10}$Be comparison

Kaplan et al. (2017) reported ten $^{26}$Al/$^{10}$Be pairs, with one sample (MAR-11-14) measured twice (Tables 2 and 4) as well as 6 pairs previously from Hagen (1995). In general, the fifteen samples do not contain substantial evidence for complex histories of burial and re-exposure (Fig. 8). Three samples (~20%) plot just below the constant exposure line at 1σ (but not at 2σ). Taken at face value, these three samples may contain evidence of burial history. In more detail: 1) MAR-11-33 gives a $^{10}$Be age of 36.4 ± 0.5 ka, which is also one the younger ages within the distribution in this part of the moraine (excluding an obvious outlier of ~12.9 ka), perhaps related to its relatively short burial history; 2) The oldest sample measured, MAR-11-14, has discordant $^{10}$Be–$^{26}$Al ages (529 ± 7, 439 ± 10, a result reproduced in the duplicate sample (532 ± 7, 455 ± 11 ka). Two possible analyses of MAR-11-14 (Fig. 8) include the following. (i) The sample plots along a line of continuous exposure but with erosion causing concentrations close to saturation. Sandstones exposed for $10^5$ years may start to disintegrate, a finding noted in earlier studies (e.g., Denton et al., 1993). (ii) Alternatively, MAR-11-14 may exhibit some history of burial, or both erosion and burial have produced the sample concentrations. The oldest sample in

Hagen (1995) may also have a similar history as MAR-11-14, with either some erosion or burial perhaps causing slightly discordant ages (at 1σ, but not 2σ).

## 5. Discussion

### 5.1. Chronology

The Mt. Achernar area preserves one of the best-dated and coherent blue-ice moraine sequences in East Antarctica. Statistically significant relations between distance and $^{10}$Be–$^{26}$Al–$^{3}$He-boron exposure ages (Fig. 7) document a net increase in exposed time from the Law Glacier margin. An exponential increase in exposure age versus distance from Law Glacier, especially for >50 ka samples (Fig. 7A), implies shorter spacing between the older ridges (Kassab et al., 2020), or an amount of original moraine morphology is less well-preserved and there are temporal gaps, or both. For deposits <50 ka, exposure age is linearly related to distance (up to 2200 m from Law ice); $r^2$ for $^{10}$Be is ~0.8.

For the oldest sectors, we infer the following based on a

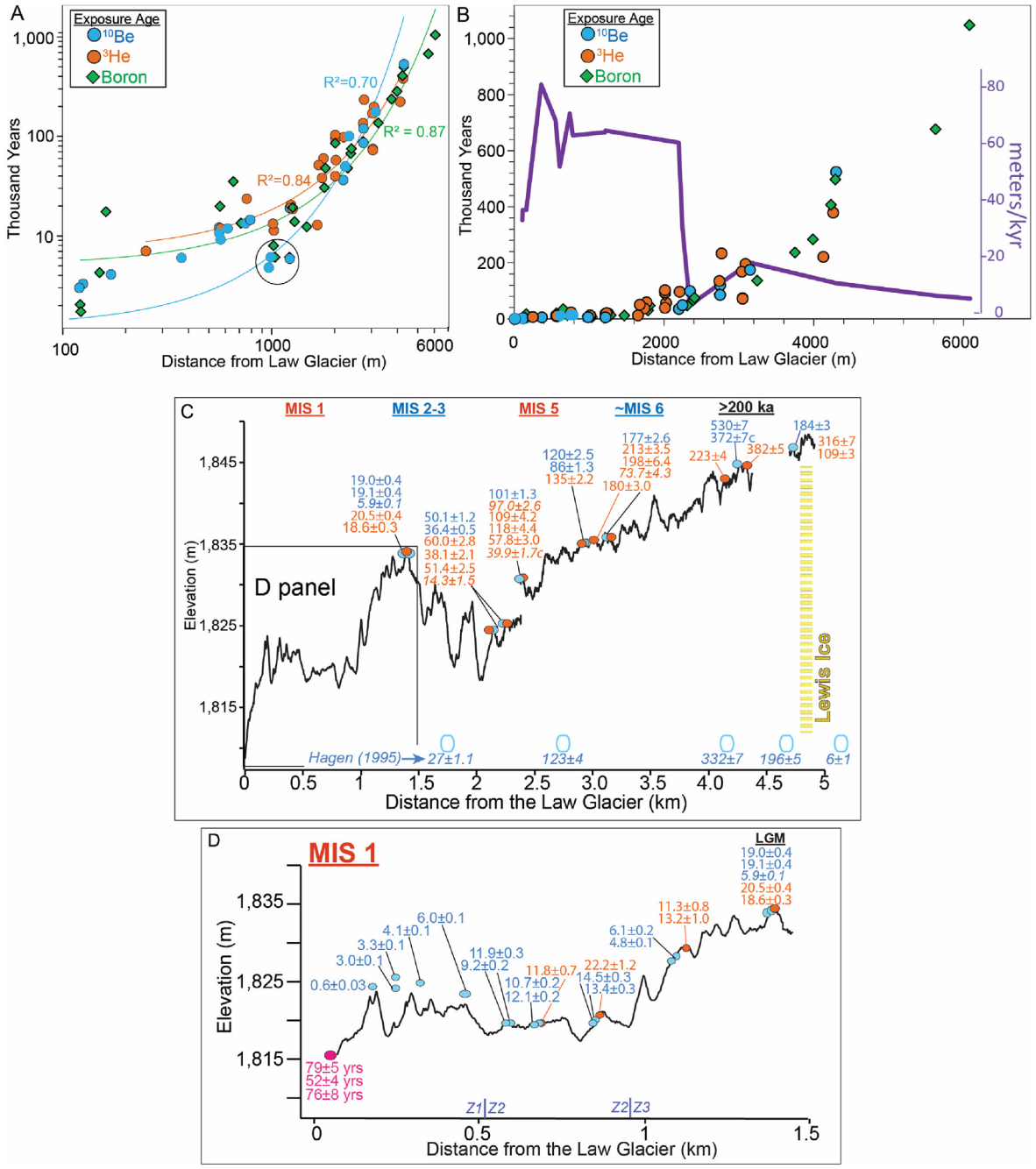


**Fig. 7.** $^{10}$Be–$^{3}$He-boron exposure ages with distance from the Law Glacier along the main transect (white-dashed line, Fig. 2). **Panels A, B**) Left side is plotted as log-log plot. Three respective exponential relations demonstrate there is a steady increase in age from the active margin. Within ~2200 m (~50 ka) from the Law Glacier, if the relation is represented by a linear line, the $r^2$ is ~0.8 ($^{10}$Be) or ~0.6 ($^{3}$He). Boron ages are from Graly et al. (2018a). Circle marks younger sediment dated, where $^{10}$Be–$^{26}$Al-boron exposure ages all indicate exposure for less time. In panel B, approximate average accretion rate based on $^{10}$Be and the two oldest boron ages at ~5600–6100 m. **Panels C, D)** Topographic profiles from Bader et al. (2017) and Kaplan et al. (2017). In panel C, the ages from Hagen (1995) are at the bottom because it is not clear how they align with the main transect. MIS labels are approximately located with distance. For simplicity, $^{26}$Al ages are not shown. In Panel D, Zones 1 to 3 (Z1-Z3) are shown along bottom.

synthesis of new and previously published findings. First, farthest from the Law Glacier, sediments have been exposed close to 500 ka, and perhaps as long as ~1 Ma (Graly et al., 2018a). The two oldest boron-exposure ages farthest from the Law Glacier in Zone 5 (southwestern sector) are ~670 ka and ~1000 ka (Figs. 2 and 7). We assume undated ridges in the southwestern and southeastern sectors of Mt. Achernar area (Figs. 1 and 2) are between ~500 ka and ~1 Ma. For the oldest Law Glacier-derived ridges in Zone 4, four cosmogenic ages (one cobble-size) and two boron ages are in the ~500-400 ka range. The oldest $^{10}$Be–$^{26}$Al sample (MAR-11-14), around 500 ka, also may be a slight underestimate for its exposure duration as the discordance between the $^{26}$Al and $^{10}$Be ages hints that some degree of erosion and/or burial led to the concentrations (Fig. 8). Our inference is consistent with Sun et al. (2015), who concluded that relatively cold dry conditions have existed since the Miocene based on the geochemistry of salts that are of subglacial origin near the Lewis Cliffs Ice Tongue margin. Second, the Lewis Cliffs Ice Tongue expanded into the Achernar moraine system, before or close to ~500 ka, given the cross-cutting relation with the dated Law moraine (yellow dashed line on Fig. 2A).

The last ~200,000 years of the moraine history is well documented by a large number of exposure ages from samples collected on quasi-continuous and often well-defined moraine ridges (Fig. 2). Sediments exposed since MIS 6 and 5 are found in both the main transect and the tail areas. Two ages are 135.2 ± 2.2 and 120.0 ± 2.5, four coherent ages provide a mean of 106 ± 9.1 ka (Section 4.1), and six ages cluster around 103.1 ± 8.9 ka (Section 4.2); a younger age of ~86 ka was found in both the main transect and tail areas, respectively. Notably, two samples associated with the ~100 ka deposits, 57.8 ± 3.0 and 39.9 ± 1.7 ka (on a cobble-size sample), overlap in age with the younger moraine ridges dated from ~55 to 35 ka. Perhaps these rocks came to the surface later (see Section 5.4), associated with localized moraine disturbance only around the sample location. The prominent lateral moraine is 9.2 ± 0.5 ka, which overlaps with the chronology in the back of Zone 1 (Figs. 3 and 7) and dates an early Holocene high in the Law Glacier surface.

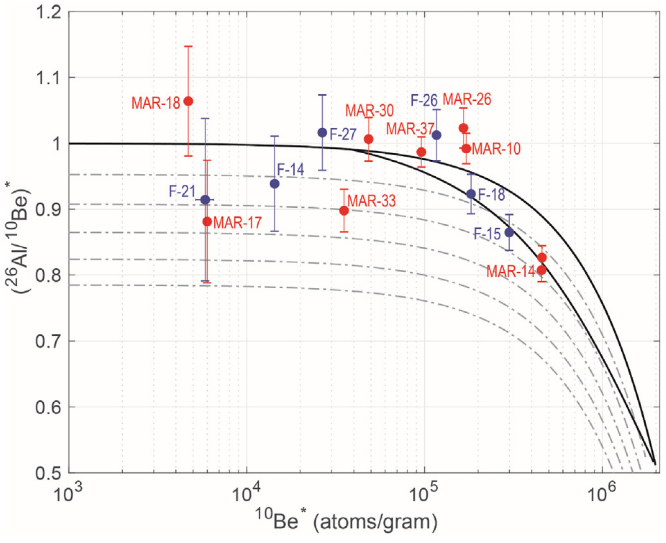


**Fig. 8.** Plot of $^{26}$Al/$^{10}$Be ratios versus $^{10}$Be concentrations, with data colored in blue and red from Hagen (1995) and Kaplan et al. (2017), respectively, recalculated with updated systematics. MAR-11-22 is not shown on the plot due to its high $^{26}$Al/$^{10}$Be value (Table 1). The first and last parts of each sample name are shown next to analyses. The ratios are standardized (*) to 6.75, the Be-10 concentrations are relative to 07KNSTD and sea level high latitude (Balco et al., 2008). Error bars are 1σ analytical uncertainty. (For interpretation of the references to color in this figure legend, the reader is referred to the Web version of this article.)

The youngest exposure ages obtained from the Law Glacier surface are <100 years for two cobble-sized samples and a boulder (Fig. 3). These three $^{10}$Be ages, as well as other analyzed samples near the tail (Fig. 5), indicate that when debris reaches the surface, it is likely to be essentially free of *in situ* cosmogenic nuclides. As nuclide production occurs even before the material reaches the surface, ages <100 years or a few centuries indicate minimal inheritance and relative rapid upward movement (to be discussed in a future paper). Moreover, the general concordance between $^{10}$Be, $^{3}$He, $^{26}$Al and boron exposure ages and their progression with distance from Law Glacier also indicates there is minimal inheritance in the moraine sediments, at least within the uncertainties of the three chronometers and overall dating of the ridges (Table 2); ~15% of the samples may have some degree of complex history, based on non-concordance with the constant exposure trajectory of $^{26}$Al/$^{10}$Be when 1σ is considered (Fig. 8). At Mt. Achernar, a lack of pre-exposure of surface material is consistent with prior studies that concluded sediment is commonly sub-glacially derived, given it is faceted and striated (Bader et al., 2017; Graly et al., 2018b).

Several ages on cobble-size samples allow for comparison with larger boulder ages. We do not find a consistent offset. Cobbles are slightly younger in some instances, although in others they are the same (near modern Law ice) or older (tail). In the back of Zone 4, a cobble next to a boulder is distinctly younger (500 ka versus 370 ka); although the younger cobble-size sample overlaps with another nearby boulder age of ~382 ka (MAR-11-13), the older sample is consistent with boron exposure ages of 500–400 kyr (Fig. 7; Graly et al., 2018a). Whether the cobble is younger because it is smaller, reached the surface later, or was affected more by periglacial processes compared with the larger boulder is unknown. Cobble-size samples were ≤5 cm thick from the side facing upwards (apparent) to its bottom (Table 1), and we processed the width of the sample, which should reduce effects of possible rotation; for the other two axes, cobble-size samples were typically also ≤5 cm 'wide,' except MAR-15-59 which is <10 cm wide. The thickness correction does not take into account, though, if the cobbles have complex histories of exposure and burial. Although as mentioned above, cobbles that were (at least) recently exposed appear to lack inherited concentrations. Additional data, including perhaps other nuclides with different half-lives, are needed to decipher the precise age of the oldest deposits, and also whether the cobble-sized materials typically afford younger ages than boulders.

A large span of the history represented in the Mt. Achernar moraine system still remains unknown. Only a handful of ridges were sampled even in the main transect (Figs. 2–5). Most of the ridges that are between ~300 ka and ~20 ka in age remain undated (Fig. 2). Between the MIS 3 (~55-35 ka) and MIS 2 (19.3 ± 0.8) dated sites, there remain ~10 unanalyzed ridges. The southwestern and southeastern sectors, which may be the oldest, and most of the tail remain unsampled.

### 5.2. Past central EAIS stability

The Achernar moraine directly chronicles past Law Glacier behavior through its internal architecture, morphology, current sediment surface elevations, and associated lateral landform (Figs. 2 and 3). These are independent measures of either quantitative or qualitative changes in ice elevation over time. Starting with internal architecture, surface sediments exposed >10 ka ($10^4$–$10^5$ yr timescale) overlie an estimated 140–190 m of debris-rich ice; and surface sediments exposed <10 ka overlie ~220 m of relatively clean ice (Kassab et al., 2020) (Figs. 3 and 9). All or most of the dated Achernar moraine thus overlies glacier ice. And, the relatively cleaner ice exposed for <10 kyr (or 20 kyr?) is linked into

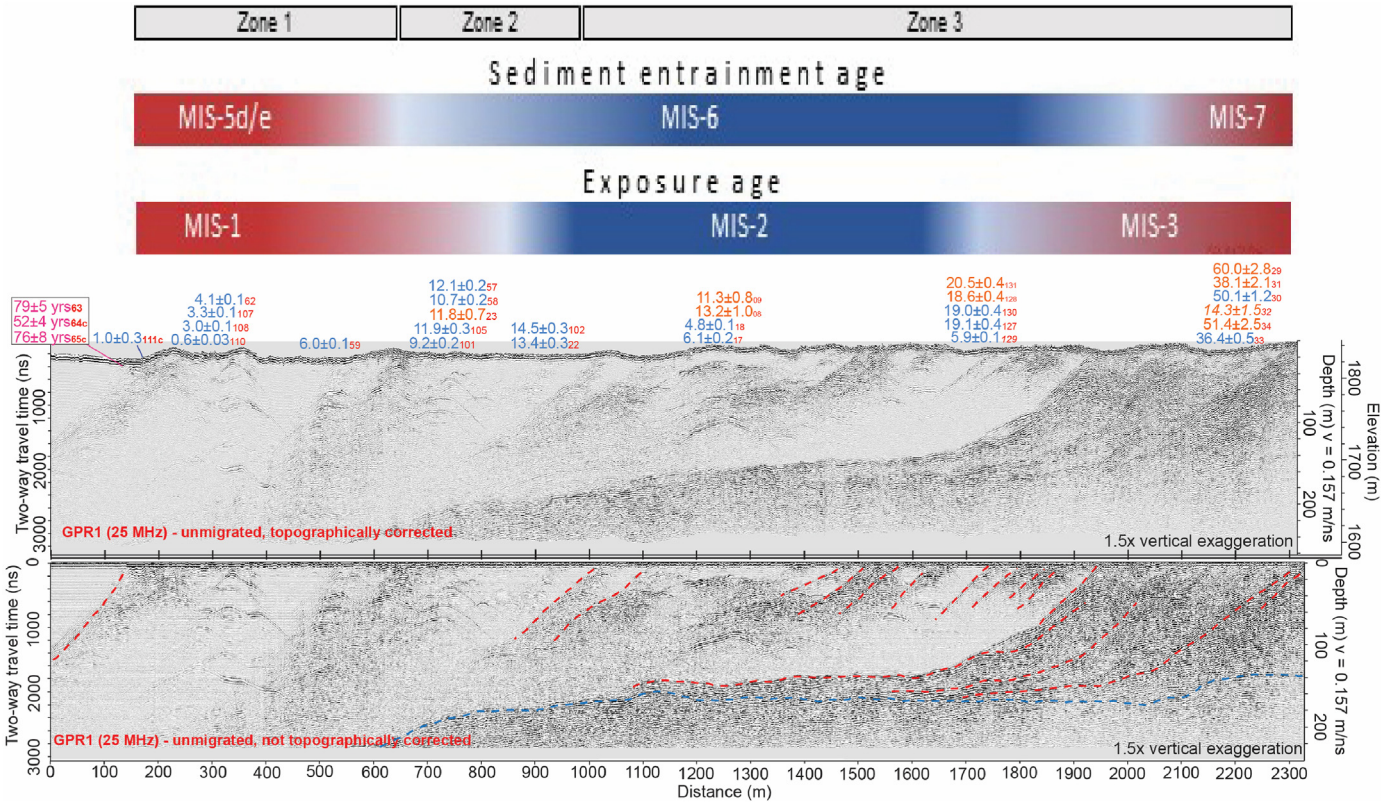


**Fig. 9.** Ground Penetrating radar (GPR, 25 MHz) with approximate locations of $^{10}$Be–$^{3}$He above the topographically corrected surface. Ages are shifted slightly so as to be at their approximate location along GPR transect. The upper panel is the processed radargram and the lower panel has interpretations including red-dashed lines as debris planes. Kassab et al. (2020) interpreted the blue-dashed line, which represents a continuous subhorizontal reflector, to be the bedrock surface at ~140 m to >220 m below. Near the top of the figure, we show both maximum sediment entrainment age (Graly et al., 2020; Kassab et al., 2020) and surface exposure ages. Boundaries between MIS #s are fuzzy given ranges of ages. Kassab et al. (2020) also presented GPR analyses for inner Zone 4, with exposure ages ≥100ka, but they found a lack of consistent GPR reflections. For simplicity, $^{26}$Al ages are not shown. (For interpretation of the references to color in this figure legend, the reader is referred to the Web version of this article.)

the core of Law Glacier. Ice and debris move upward, with the latter focused along debris bands that are connected to the topographic highs that are moraine ridges (Figs. 3 and 9) (Kassab et al., 2020). In this way, the Achernar site is analogous to other Antarctic blue-ice moraine sediment areas (e.g., Campbell et al., 2013; Hein et al., 2016; Akçar et al., 2020; Woodward et al., 2022).

An important consequence of the aforementioned structure below the moraines is that if, or when, the surface of Law Glacier lowers substantially it would disturb the moraine architecture, including the well-defined geomorphology and the long, mostly continuous parallel/sub-parallel ridges and troughs that contain sediments exposed for $10^4$–$10^5$ years (Figs. 3–5). In a scenario whereby the buttressing support of Law Glacier ice is removed, it would cause surface slopes to be reversed and, eventually, drawdown of the blue-ice sediment ridges. Woodward et al. (2022) described such a scenario in the Heritage Range, West Antarctica, where thinning and a reversal of flow occurred in a blue-ice moraine setting. Previously, based on the till characteristics and provenance, Bader et al. (2017) concluded that the debris sources of the Mt. Achernar sediments were relatively constant over time, which indicates relative stability of the central EAIS.

Our findings, as well as those in prior studies (e.g., Scarrow et al., 2014; Bader et al., 2017) raise questions including: (1) When did the preserved sediments first start to collect? (2) When and how was the Mt Achernar blue-ice moraine disturbed, in ways that are recorded in its geomorphology and chronology, which reflect major changes in paleoglaciology? On the first question, as discussed above, we infer the oldest part of the moraine (Fig. 2) is at least 500-400 ka and perhaps close to 1 Ma. Additional data are needed to evaluate further when the sediment started to collect. On the second question, we infer that an important disturbance occurred when the Lewis Cliffs Ice Tongue grew and impinged on the main area (Fig. 2A). Lewis Ice disturbed the Achernar moraine, close to or before 500-400 ka. The timing may be before or during MIS 11 (*424,000 to 374,000 years*). With one exception, the oldest exposure ages in the back of Zone 4 are around or younger than MIS 11. Moreover, we note that the 500-300 ka ages in the back of Zone 4 decrease by about 10% and lie in the ~450-300 ka range (Table 2) if the LSDn scaling method (Lifton et al., 2014) and a lower production rate are more appropriate for use in high latitudes and on older surfaces in Antarctica (Balter-Kennedy et al., 2020). If correct, the findings imply slightly higher central EAIS surfaces during or before MIS 11, at least associated with the Lewis Cliffs Ice Tongue. In comparison, Blackburn et al. (2020) recently inferred an MIS 11 impact to the central EAIS, specifically recession around the Wilkes Basin. Another disturbance to the Achernar moraine morphology is recorded by the age discontinuity in the tail area, as much of a glacial cycle appears missing between the grey lateral moraine and the oxidized till, which is discussed more below.

### 5.3. Past Law Glacier surfaces

At Mt. Achernar, the magnitude of glacier surface changes that disturb moraine architecture is an outstanding question. Relatively minor surface elevation changes occurred at the heads of central TAM outlet glaciers, including thinning during much of the middle-late Holocene (cf., Mercer, 1968; Denton et al., 1989; Todd et al., 2010; Bromley et al., 2012; Hall et al., 2013), as also documented

here. At Mt. Achernar, disturbances to the blue-ice moraine may depend on the rate as well as the magnitude of surface elevation changes, especially relative to the subglacial bedrock elevations. We infer minimal changes in the magnitude of glacier surface elevation over (at least) the time periods in which dated sediments are preserved. Surface elevational changes over the last ~500-400 kyr must have been minor enough to have left "intact" Zones 3 and 4 ($10^4$–$10^5$ yrs).

The following estimates for past surface changes around the Mt. Achernar blue-ice moraine are based on several observations. First, the far-maximum possible elevational drop (thinning) from the current ice surface is ~150 m, which is depth of the underlying bedrock ridge (Kassab et al., 2020). We conclude that such a decrease has not occurred, otherwise debris would have been removed from the Mt. Achernar moraine sequence. Second, a minimum of ~50 m of widespread ice surface elevation change is needed to disturb the moraine, following Bader et al. (2017). The right lateral moraine along the headwall of Mt. Achernar shown in Fig. 6D–F indicates ~40–50 m of thickening close to the present Law Glacier at ~10-9 ka (Bader et al., 2017). We assume the right lateral moraine formed alongside the margin of a slightly expanded Law Glacier, as it flowed off the plateau along Mt. Achernar. For about 0.5–1 km distance inward the Achernar moraine appears relatively disturbed (see yellow lines on Fig. 6G), although some semblance of moraine ridges and troughs still exist (Kassab et al., 2020). Thus, the high glacier surface at ~10-9 ka and subsequent drop appears to have modified only a small area of the Achernar moraine system close to the headwall. As the lateral moraine descends (southeastward) away from Law Glacier and ends, the Mt. Achernar moraine regains a well-preserved ridge and trough form (Fig. 6G).

Above the lateral moraine, a trimline (Figs. 3 and 6) exists that separates material of different relative weathering and indicates a higher ice surface before ~9.2 ka. We estimate that it is ~15–20 m and <10 m above the lateral moraine, near MAR-15-92 and −96, respectively. These may be minimum estimates given the slope and rockfall (Fig. 6E and F). As the trimline is on a steep scree slope, we did not collect samples for exposure dating. Implications of the higher, undated trimline are as follows. First, if the trimline is older than or around ~500-400 ka, its age may reflect thickening of Law Glacier at the same time as the Lewis Cliffs Ice Tongue expanded (Section 5.1). Second, if the trimline is <500-400 ka in age, then its occurrence indicates ice surface elevations may have been higher by a minimum of ~70 m near MAR-15-92 (~50 m for the lateral moraine plus ~20+ m to the trimline) and ~10–20 m (i.e., above the blue-ice moraine) near MAR-15-96. If the trimline is <500-400 ka in age, such increased (and then decreased) ice surface changes still did not disturb more than a relatively small area (Figs. 2 and 6G), and the blue-ice moraine system still remained buttressed by Law Glacier.

A third line of evidence for relatively limited surface changes associated with preserved moraine comes from the tail area, where the elevation of the oxidized sediments dated to MIS 6 and MIS 5 is similar to the present Law surface (Fig. 5), ~1750-1740 m. The grey-colored or unoxidized moraine, dated from ~18 ka to ~1 ka, is about 5–10 m higher than the present Law Glacier surface; this change, albeit possibly a minimum, did not disturb older, ≥100 ka deposits that are only ~300 m away.

Fourth, changes of ≤30 m since MIS 2 across a widespread sector of the main area of the Achernar moraine also did not disturb the older Zone 3 and 4 ridges shown in Figs. 2 and 4. The precise amount of current elevational change across the moraine varies depending on where measured, which perhaps reflects localized processes or effects (Figs. 3 and 7), such as sub-surface ice behavior including relative to bedrock depth. The ~20-19 ka section of the moraine is about ~20–25 m above the current Law Glacier surface, perhaps indicating higher ice input during the global LGM. From ~14 to ~10 ka, there may have been relatively less ice input into the moraine (Bader et al., 2017). Ice input then increased by ~9.2 ka, when the lateral moraine formed.

We note the net or steady rise in the moraine surface with distance from the Law Glacier, shown in Fig. 7. The back of Zone 4 is about 40 m above the present ice surface, before the topography declines back towards Lewis Cliffs Ice Tongue. We assume the increasing subglacial bedrock elevations along with the englacial flow (Kassab et al., 2020) allow sediment-moraine surface elevations to increase slightly, away from the buttressing Law Glacier. The insulation of the overlying sediment, which reduces sublimation as it thickens (Lamp and Marchant, 2017), may also allow slightly higher surfaces away from Law ice (Figs. 7 and 9).

### 5.4. Blue-ice moraine processes including formation

The chronology allows us to build upon prior studies at Mt. Achernar (Scarrow et al., 2014; Bader et al., 2017, Graly et al., 2018a,b, 2020; Kassab et al., 2020), to improve our understanding of blue-ice areas and associated processes, refine conceptual models, and to raise new questions. Any conceptual model needs to account for the increase in surface exposure age and till thickness with distance from Law Glacier, change in sediment concentration in subsurface ice, and how new sediment ridges form at the Law edge-moraine margin (Figs. 2–7, 9).

In the main moraine area, the debris concentration in the englacial ice is substantially greater below sediment surfaces exposed longer than 50 ka, compared with younger parts of the moraine (Fig. 9). Below sediment surfaces exposed >50 ka, there is a lack of distinct GPR reflections; Kassab et al. (2020) hypothesized the amount of subsurface debris becomes high enough that GPR reflections interfere with each other and no individual hyperbolic reflections are therefore observed. In association with the large ridges, especially for those exposed ~50-35 kyr, the dipping reflections appear to cluster and merge. Kassab et al. (2020) inferred that underlying the innermost moraine (Fig. 3, Zones 1 and 2) the lack of reflections indicates clean ice or that with low debris concentration given the resolution (Fig. 9).

The chronology tied to the GPR-based findings lead us to infer that a significant change in englacial sediment concentration occurred around or by ~50 ka, which was caused, at least in part, by even earlier changes in basal entrainment (Fig. 9). For moraine exposed longer than 50 kyr, we infer slower subsurface ice velocity including upward movement (Fig. 9; Kassab et al., 2020), compared with that under younger parts of the moraine. Till thicknesses of ~15 cm to >1 m associated with exposure ages >20 ka (Scarrow et al., 2014; Bader et al., 2017) are consistent with slower rates of subsurface ice velocities. As till thickness increases, sublimation is reduced and eventually may be effectively shut off (Lamp and Marchant, 2017). Sublimation helps drive ice upwards (Whillans and Cassidy, 1983), hence, as its rate declines under thickening sediment 'horizontal' and upward ice velocities should decrease or essentially stop. In contrast, till thickness <10 cm are associated with the youngest Zone 1 sediments (Bader et al., 2017), where the subsurface ice is relatively clean and moraine is still forming.

The $^{10}$Be–$^{3}$He–$^{26}$Al-boron exposure ages allow us to refine an apparent sequential lateral accretion rate, as new ridges formed at the moraine-Law Glacier margin (Kassab et al., 2020). The accretion age may be similar to surface exposure age, and both may differ substantially from the ice and sediment entrainment age (Fig. 9) (Graly et al., 2018b). We confirm the apparent rate of debris accumulation and lateral growth has not been constant over time (Fig. 7B). The fastest estimated rates of lateral accretion, >60 m/kyr, are associated with a distance of ~800-400 m from the margin or roughly the ~15-5 ka exposed interval. Average rates >50 m/kyr are

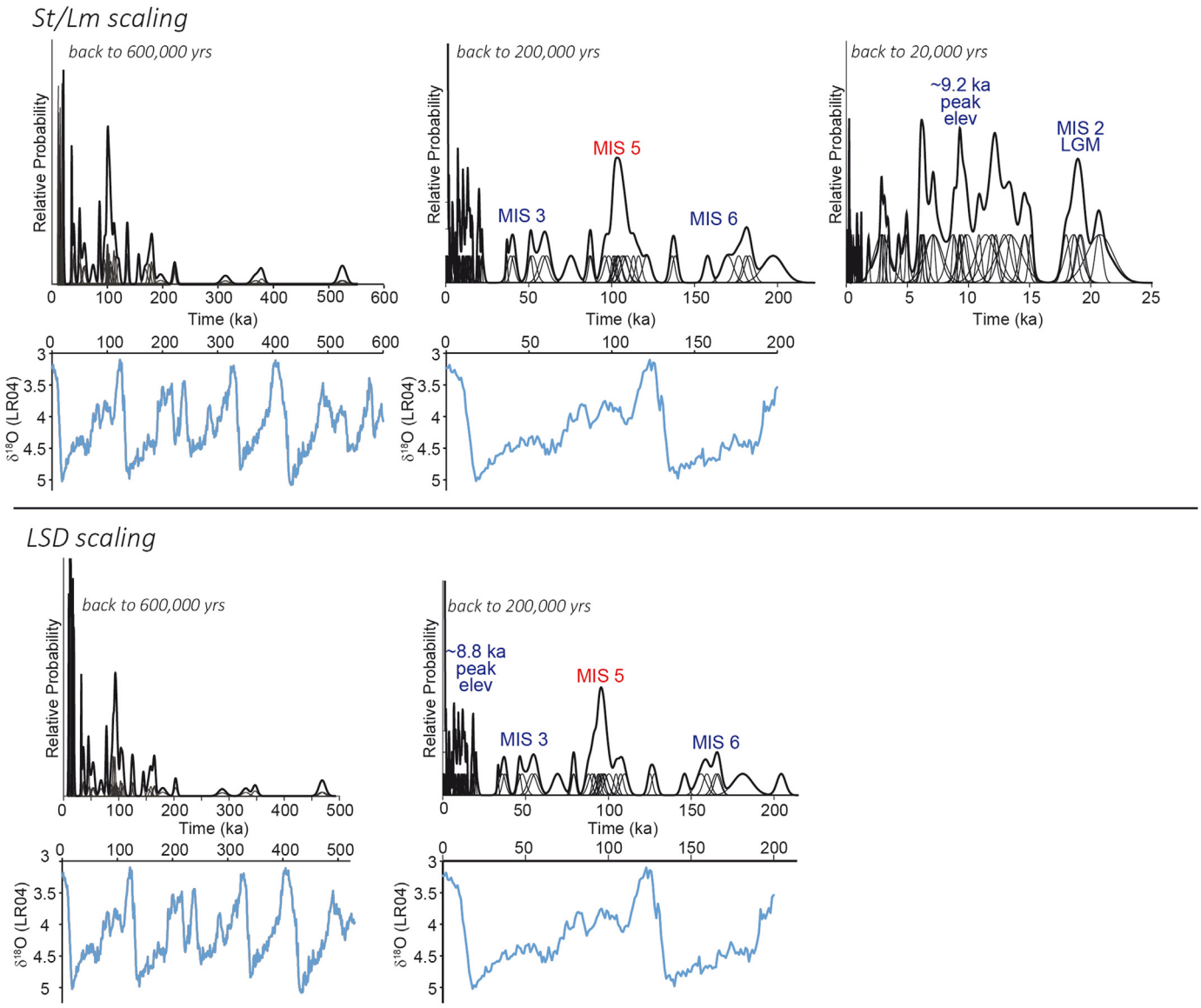


**Fig. 10.** $^{10}$Be–$^{26}$Al–$^{3}$He ages compared with benthic $\delta^{18}$O stack (Lisiecki and Raymo, 2005). Top panels include ages with St/Lm scaling (difference not discernible at the scale shown). For MIS 5, a concentration of ages occurs at 120-100 ka excluding "outlier' ages <90 ka from the same sites (Fig. 5). Bottom panels include exposure ages calculated with the LSDn scaling (Tables 1 and 3) method, which are ~10–12% lower than those calculated based on St/Lm.

generally characteristic of the inner 2000 m or last ~50 kyr. For moraine exposed from ~50 ka to 1 Ma, there is a net decrease and then relatively constant and low apparent accretion rate, which is reflected in the exponential relation between ages and distance from the margin (Fig. 7A). Additional analyses are needed on ridges >50 ka to determine whether decreased apparent accretion rates reflect gaps in preservation or the moraine becoming spatially compressed, or both.

Down flow from Mt. Achernar, the tail area records a different history than the main area studied. The overall form of the tail is parallel or quasi-parallel with the current Law Glacier flow direction (Figs. 1 and 2A). We infer that formation of the tail has been influenced by prevailing ice flow direction in a different manner than that of the main area (Fig. 1C and D). Furthermore, although well-developed moraine ridges exist, particularly that associated with the grey unoxidized till, they are not as prominent throughout the older parts of the tail as they are in the main area (Fig. 2). Some ridges in the tail are at a different orientation and appear cross-cut by the young grey moraine. In addition, there is an age discontinuity in the tail area of ~60–80 kyr, which does not appear in the main area. For now, we speculate a change in ice thickness occurred in relation to the subglacial bed elevation, which altered the spatial pattern of debris entrainment between the tail and main transect area closer to Mt. Achernar. Perhaps a shallow subglacial bedrock ridge exists between the main area and the tail that shifted the accretion pattern as ice thickness changed, even by relatively minor amounts. However, additional geophysical (e.g., GPR) and chronological observations are needed to understand why in the downstream tail area the discontinuity exists during the last glacial cycle.

Under particular conditions, blue-ice moraines can develop towards equilibrium forms (D. Sugden personal communication). Over time, sublimation causes a progressive loss of glacier ice and thickening of surface sediments, which is documented for moraine exposed for >50 ka in the main area at Mt. Achernar. Continued compressive glacier flow also may increase the concentration of debris and perhaps ridges in older parts of the blue-ice moraine (e.g., Fig. 7). Younger samples within an otherwise relatively coherent older population (Section 5.1, 'so-called outliers'), or

variability in exposure ages, might be expected if sublimation caused a boulder or cobble to reach the surface long after (most of?) the moraine formed; resulting exposure age variability may be due to active subsurface debris planes. Individual samples also may be younger because localized periglacial activity caused them to move downward or rotate, and later re-emerge at the surface. Our inferences are consistent with others' conclusions elsewhere in Antarctica (e.g., Fogwill et al., 2012; Ackert et al., 2013; Hein et al., 2016; Woodward et al., 2022).

### 5.5. Comparison with global ice sheet changes

We display our results alongside the benthic $\delta^{18}O$ record, which allows comparisons between exposure ages and past global climate and ice sheet changes (Lisiecki and Raymo, 2005) (Fig. 10). Given that most ridges are not yet dated we highlight again, especially for older parts of the Achernar moraine sequence, inferences are tentative as only parts of its history are known. The findings imply slightly higher central EAIS surfaces during or before MIS 11, at least to cause growth of the Lewis Cliffs Ice Tongue. Moraine ridges not yet dated may reveal an MIS 4 (cf., Doughty et al., 2021) part of the sequence. As MIS 5 ages are found both in the main and tail areas, and considering the well-preserved geomorphology formed during MIS 1 (<11.8 ka), the findings imply other prior interglacial periods also might be well-represented in the Mt. Achernar moraine. In fact, despite sampling only a small number of ridges in the main area and a small part of the tail, the distributions of MIS 5 ages obtained overlap statistically, ~105-100 ka (Lm, LSDn ages are ~10% lower). Exposure ages between ~100 and 80 ka imply all of MIS 5 may be represented at Mt. Achernar.

The time since MIS 2 is well documented, given sampling was comprehensive (Fig. 10). There are no exposure ages overlapping with the first half of Termination I, when ice receded globally (Denton et al., 2010, 2021), except for one $^{26}Al$ age that is high relative to its paired $^{10}Be$ analysis (MAR-11-22). Perhaps there was less sediment delivery during peak Termination periods, which is also consistent with the conclusion of Kassab et al. (2020) that colder global periods have higher debris concentration and entrainment. Such changes in sediment concentration may correspond to ice flow history relative to loci of entrainment, with closer sources leading to higher concentrations. However, given the lack of ridges dated, such inferences need to be tested with additional analyses. A high surface elevation around 9.5–9 ka is consistent with other interior EAIS studies that observed thick ice during the early Holocene, perhaps associated with a lag response to downstream dynamics or increased accumulation on the plateau (e.g., Hall et al., 2013).

## 6. Conclusions and questions

Blue-ice moraine sediments at Mt. Achernar in the central Transantarctic Mountains offer at least ~500-400 ka and likely ~1 Ma of paleoglaciologic history of the edge of the EAIS plateau. Blue-ice moraines represent — for time periods in which they are preserved — relatively constant EAIS outlet glacier conditions and quasi-equilibrium forms. A relatively stable central EAIS occurred during MIS 5, in terms of ice surface elevation, which left older MIS 6+ geomorphology and sediments intact. Our findings are consistent with those of other blue-ice studies around Antarctica (e.g., Fogwill et al., 2012). Disturbances to the Achernar blue-ice moraine did occur, but the magnitude of change was limited. The largest obvious disturbance was when the nearby Lewis Cliffs Ice Tongue was expanded, close to or prior to 500-400 ka. Gaps in the blue-ice moraine record may be more evident prior to the last two glacial cycles. The observations support surface elevation changes associated with the Law Glacier of a minimum of ~50 m over at least the last two glacial cycles. A slight increase in ice thickness or ice input seems associated with the global LGM around ~20 ka and during the earliest Holocene, 9.2 ± 0.5 ka. Sediments that recently reached the Law Glacier surface contain negligible inheritance in the context of the older moraine dating.

We ask the following questions specifically in terms of the Mt. Achernar record. However, the answers will provide a better context and understanding of blue-ice moraines as important paleoglaciologic archives around Antarctica. When did sediments start to accumulate at Mt. Achernar? What magnitude and rate of surface change disturbs moraine architecture, especially relative to subglacial flow and bedrock elevation? What caused the Lewis Cliffs Ice Tongue to expand and disturb the Law Glacier moraine sequence, and was it due to MIS 11 local climatic conditions? What caused debris to increase substantially below surfaces exposed >20 ka, and especially >50 ka, and are these particular times random? What determines the location of debris-loaded bands or planes? We infer ridge preservation and location of debris planes may be due to glacier surface history, how basal material is sub-glacially entrained, and thereafter how flow occurs relative to bedrock topography and structure. Another possibility is that englacial concentrations are dependent on where debris is derived, perhaps at specific places along the bed, with higher amounts associated with closer sources. Future modeling-based studies can also provide additional insights into blue-ice moraine processes.

## Author contribution

Kaplan, Licht, Winckler, Schaefer, Graly: Conceptualization. **All authors,** Investigation, Writing-Reviewing and Editing.

## Declaration of competing interest

The authors declare that they have no known competing financial interests or personal relationships that could have appeared to influence the work reported in this paper.

## Data availability

The data are in this manuscript and provided as supplementary tables.

## Acknowledgements

This work was supported by National Science Foundation Antarctic grants PLR-1443433, PLR-1443213, ANT-0944578 and ANT-0944475. JMS acknowledges support by the Vetlesen Foundation. We thank the Polar Geospatial Center and UNAVCO (Marianne Okal, Annie Zaino, Joe Petit), the US Antarctic Program, Kenn Borek Air, Ltd., Michael Roberts and Peter Braddock and all other field team members from the 2010/11 and 2015/16 seasons. We also thank all personnel at the Center of Accelerator Mass Spectrometry (CAMS) at Lawrence Livermore National Laboratory and PRIME Lab for analyses. We thank Jean Hanley and Jeremy Frisch for laboratory assistance. As Reviewers, David Sugden and Peter Almond substantially improved the clarity and strength of the manuscript.

## References

Akçar, N., Yeşilyurt, S., Hippe, K., Christl, M., Vockenhuber, C., Yavuz, V., Özsoy, B., 2020. Build-up and chronology of blue ice moraines in QueenMaud Land, Antarctica. Quat. Sci. Adv. 2, 100012.

Ackert, R.P., 2000. Antarctic Glacial Chronology: New Constraints from Surface Exposure Dating, PhD Thesis. Woods Hole Oceanographic Institution, Massachusetts Institute of Technology, p. 213.

Ackert Jr., R.P., Putnam, A.E., Mukhopadhyay, S., Pollard, D., DeConto, R.M.,

Kurz, M.D., Borns Jr., H.W., 2013. Controls on interior West Antarctic Ice Sheet elevations: inferences from geologic constraints and ice sheet modeling. Quat. Sci. Rev. 65, 26–38. https://doi.org/10.1016/j.quascirev.2012.12.017.
Bader, N.A., Licht, K.J., Kaplan, M.R., Kassab, C., Winckler, G., 2017. East Antarctic ice sheet stability recorded in a high-elevation ice-cored moraine. Quat. Sci. Rev. 159, 88–102.
Balco, G., Stone, J.O., Lifton, N.A., Dunai, T.J., 2008. A complete and easily accessible means of calculating surface exposure ages or erosion rates from $^{10}$Be and $^{26}$Al measurements. Quat. Geochronol. 3, 174–195.
Balco, G., 2020. Noncosmogenic helium-3 in pyroxene and antarctic exposure dating. https://cosmognosis.wordpress.com/2020/08/22/noncosmogenic-helium-3-in-pyroxene-and-antarctic-exposure-dating/.
Balter-Kennedy, A., Bromley, G., Balco, G., Thomas, H., Jackson, M.S., 2020. A 14.5-million-year record of East Antarctic ice sheet fluctuations from the central transantarctic Mountains, constrained with cosmogenic $^{3}$He, $^{10}$Be, $^{21}$Ne, and $^{26}$Al. Cryosphere 14, 2647–2672. https://doi.org/10.5194/tc-14-2647-2020.
Bintanja, R., 1999. On the glaciological, meteorological and climatological significance of Antarctic blue ice area. Rev. Geophys. 37, 337–359.
Blackburn, T., Edwards, G., Tulaczyk, S., Scudder, M., Piccione, G., Hallet, B., McLean, N.M., Zachos, J., Cheney, B., Babbe, J., 2020. Ice retreat in Wilkes basin of east Antarctica during a warm interglacial. Nature 583 (i), 7817.
Borchers, B., Marrero, S., Balco, G., Caffee, M., Goehring, B., Lifton, N., Nishiizumi, K., Phillips, F., Schaefer, J., Stone, J., 2016. Geological calibration of spallation production rates in the CRONUS-Earth project. Quat. Geochronol. 31, 188–198.
Bromley, G.R.M., Hall, B.L., Stone, J.O., Conway, H., 2012. Late Pleistocene evolution of Scott Glacier, southern Transantarctic Mountains: implications for the Antarctic contribution to deglacial sea level. Quat. Sci. Rev. 50, 1–13.
Bromley, G.R.M., Winckler, G., Schaefer, J.M., Kaplan, M.R., 2014. Pyroxene separation by HF leaching and its impact on helium isotopes. Quat. Geochronol. 23, 1–8.
Campbell, S., Balco, G., Todd, C., Conway, H., Huybers, K., Simmons, C., Vermeulen, M., 2013. Radar-detected englacial stratigraphy in the Pensacola Mountains, Antarctica: implications for recent changes in ice flow and accumulation. Ann. Glaciol. 54, 91–100.
Cassidy, W., Harvey, R., Schutt, J., Disle, G., Yanai, K., 1992. The meteorite collection sites of Antarctica. Meteoritics 27, 490–525. https://doi.org/10.1111/j.1945-5100.1992.tb01073.x.
Chinn, T.J., 1991. Polar glacier margin and debris features. Memor. Soc. Geol. Ital. 46, 25–44.
Chinn, T.J., 1994. Glacier Disequilibrium in the Convoy Range, Transantarctic Mountains, Antarctica, vol. 217. Institute of Geological & Nuclear Sciences Contribution, pp. 269–276.
Corti, G., Zeoli, A., Belmaggio, P., Folco, L., 2008. Physical modeling of the influence of bedrock topography and ablation on ice flow and meteorite concentration in Antarctica. J. Geophys. Res. 113 (F1). https://doi.org/10.1029/2006JF000708.
DeConto, R.M., Pollard, D., 2016. Contribution of Antarctica to past and future sea-level rise. Nature 531, 591–597. https://doi.org/10.1038/nature17145.
Denton, G.H., Bockheim, J.G., Wilson, S.C., Leide, J.E., 1989. Late quaternary ice surface fluctuations of beardmore glacier, transantarctic Mountains. Quat. Res. 31, 183–209.
Denton, G.H., Anderson, R.F., Toggweiler, J.R., Edwards, R.L., Schaefer, J.M., Putnam, A.E., 2010. The last glacial termination. Science 328, 1652–1656.
Denton, G.H., Sugden, D.E., Marchant, D.R., Hall, B.L., Wilch, T.I., 1993. East Antarctic ice sheet sensitivity to pliocene climatic change from a dry valleys perspective. Geografiska Annaler Series A 75, 155–204.
Denton, G.H., Putnam, A.E., Russell, J.L., Barrell, D.J.A., Schaefer, J.M., Kaplan, M.R., Strand, P.D., 2021. The Zealandia Switch: ice age climate shifts viewed from Southern Hemisphere moraines. Quat. Sci. Rev. 257, 106771.
Doughty, A.M., Kaplan, M.R., Peltier, C., Barker, S., 2021. A global maximum in glacier extent during MIS 4. Quat. Sci. Rev. 261, 106948.
Eaves, S.R., Winckler, G., Schaefer, J.M., Vandergoes, M.J., Alloway, B.V., Mackintosh, A.N., Townsend, D.B., Ryan, M.T., Li, X., 2015. A test of the cosmogenic 3He production rate in the south-west Pacific (39°S). J. Quat. Sci. 30, 79–87.
Eaves, S.R., Mackintosh, A.N., Winckler, G., Schaefer, J.M., Alloway, B.V., Townsend, D.B., 2016. A Cosmogenic $^{3}$He chronology of late Quaternary glacier fluctuations in North Island, New Zealand (39°S). Quat. Sci. Rev. 132, 40–56.
Faure, G., Mensing, T.M., Johnson, K.S., 1992. Composition of rock clasts in the Mt. Achernar moraine and the Lewis Cliff ice tongue. Antarct. J. U. S. 11–12.
Fogwill, C.J., Hein, A.S., Bentley, M.J., Sugden, D.E., 2012. Do blue-ice moraines in the Heritage Range show the West Antarctic ice sheet survived the last interglacial? Palaeogeogr. Palaeoclimatol. Palaeoecol. 335–336, 61–70.
Golledge, N.R., 12 others, 2013. Glaciology and geological signature of the last glacial maximum antarctic ice sheet. Quat. Sci. Rev. 78, 225–247.
Graly, J.A., Licht, K.J., Drushel, G.K., Kaplan, M.R., 2018a. Polar desert chronologies through quantitative measurements of salt accumulation. Geology 46, 351–354.
Graly, J.A., Licht, K.J., Kassab, C.M., Bird, B.W., Kaplan, M.R., 2018b. Warm-based basal sediment entrainment and far-field Pleistocene origin evidenced in central Transantarctic blue ice through stable isotopes and internal structures. J. Glaciol. 64, 185–196.
Graly, J.A., Licht, K.J., Bader, N.A., Bish, D.L., 2020. Chemical weathering signatures from Mt. Achernar Moraine, Central Transantarctic Mountains I: subglacial sediments compared to underlying rock. Geochem. Cosmochim. Acta 283, 149–166.
Hagen, E.H., 1995. A Geochemical and Petrological Investigation of Meteorite Ablation Products in till and Ice of Antarctica [Ph.D. Thesis]. The Ohio State University, Columbus, p. 525.
Hall, B.L., Denton, G.H., Stone, J.O., Conway, H., 2013. History of the Grounded Ice Sheet in the Ross Sea Sector of Antarctica during the Last Glacial Maximum and the Last Termination, vol. 381. Geological Society, London, pp. 167–181. Special Publication.
Hein, A., et al., 2016. Evidence for the stability of the west antarctic ice sheet divide for 1.4 million years. Nat. Commun. 7, 10325–10332. https://doi.org/10.1038/ncomms10325.
Higgins, J.A., Kurbatov, A.V., Spaulding, N.E., Brook, E., Introne, D.S., Chimiak, L.M., Yan, Y., Mayewski, P.A., Bender, M.L., 2015. Atmospheric composition 1 million years ago from blue ice in the Allan Hills, Antarctica. Proc. Natl. Acad. Sci. USA 112, 6887–6891.
Howat, I.M., Porter, C., Smith, B.E., Noh, M.-J., Morin, P., 2019. The reference elevation model of Antarctica. Cryosphere 13, 665–674. https://doi.org/10.5194/tc-13-665-2019.
Joy, K., Fink, D., Storey, B., Atkins, C., 2014. A 2 million year glacial chronology of the hatherton glacier, Antarctica and implications for the size of the east antarctic ice sheet at the last glacial maximum. Quat. Sci. Rev. 83, 46–57.
Kaplan, M.R., Strelin, J.A., Schaefer, J.M., Denton, G.H., Finkel, R.C., Schwartz, R., Putnam, A.E., Vandergoes, M.J., Goehring, B.M., Travis, S.G., 2011. In-situ cosmogenic $^{10}$Be production rate at Lago Argentino, Patagonia: implications for late-glacial climate chronology. Earth Planet Sci. Lett. 309, 21–32.
Kaplan, M.R., Licht, K.J., Winckler, G., Schaefer, J.M., Bader, N., Mathieson, C., Roberts, M., Kassab, C.M., Schwartz, R., Graly, J.A., 2017. Mid-late pleistocene stability of the central East antarctic ice sheet at the head of Law Glacier. Geology 45, 963–966.
Kassab, C.M., Licht, K.J., Petersson, R., Lindbäck, K., Graly, J.A., Kaplan, M.R., 2020. Formation and evolution of an extensive blue ice moraine in central Transantarctic Mountains, Antarctica. J. Glaciol. 66, 49–60.
Lal, D., 1991. Cosmic-ray labeling of erosion surfaces in-situ nuclide production rates and erosion models. Earth Planet Sci. Lett. 104, 424–439.
Lamp, J.L., Marchant, D.R., 2017. Vapor transport and sublimation on mullins glacier, Antarctica. Earth Planet Sci. Lett. 465, 82–91.
Lisiecki, L.E., Raymo, M.E., 2005. A Pliocene-Pleistocene stack of 57 globally distributed benthic delta O-18 records. Paleoceanography 20.
Lifton, N., Sato, T., Dunai, T., 2014. Scaling in situ cosmogenic nuclide production rates using analytical approximations to atmospheric cosmic-ray fluxes. Earth Planet Sci. Lett. 386, 149–160.
Mercer, J.H., 1968. Glacial geology of the Reedy glacier area, Antarctica. Geol. Soc. Am. Bull. 79, 471–486.
Palmer, E.F., Licht, K.J., Swope, R.J., Hemming, S.R., 2012. Nunatak moraines as a repository of what lies beneath the East Antarctic ice sheet. In: Rasbury, E.T., Hemming, S.R., Riggs, N.R. (Eds.), Mineralogical and Geochemical Approaches to Provenance, 487. Geological Society of America Special Paper, pp. 97–104.
Pattyn, R., 2010. Antarctic subglacial conditions inferred from a hybrid ice sheet/ice stream model. Earth Planet Sci. Lett. 295, 451–461.
Putnam, A., Schaefer, J., Barrell, D.J.A., Vandergoes, M., Denton, G.H., Kaplan, M., Finkel, R.C., Schwartz, R., Goehring, B.M., Kelley, S., 2010. In situ cosmogenic $^{10}$Be production-rate calibration from the Southern Alps, New Zealand. Journal of Quaternary Geochronology 5, 392–409.
Scarrow, J.W., Balks, M.R., Almond, P.C., 2014. Three soil chronosequences in recessional glacial deposits near the polar plateau, in the Central Transantarctic Mountains, Antarctica. Antarct. Sci. 26, 573–583.
Schäfer, J.M., Ivy-Ochs, S., Wieler, R., Leya, I., Baur, H., Denton, G.H., Schlüchter, C., 1999. Cosmogenic noble gas studies in the oldest landscape on earth: surface exposure ages of the Dry Valleys, Antarctica. Earth Planet Sci. Lett. 167, 215–226.
Schaefer, J.M., Denton, G.D., Kaplan, M.R., Putnam, A., Finkel, R.C., Barrell, D.J.A., Andersen, B.G., Schwartz, R., Mackintosh, A., Chinn, T., Schlüchter, C., 2009. High frequency Holocene glacier fluctuations in New Zealand differ from the northern signature. Science 324, 622–625.
Sinisalo, A., Moore, J.C., 2010. Antarctic blue ice areas – towards extracting paleoclimate information. Antarct. Sci. 22, 99–115.
Stone, J.O., 2000. Air pressure and cosmogenic isotope production. J. Geophys. Res. 105, 23753–23759.
Sun, T., Socki, R.A., Bish, D.L., Harvey, R.P., Bao, H., Niles, P.B., Cavicchioli, R., Tonui, E., 2015. Lost cold Antarctic deserts inferred from unusual sulfate formation and isotope signatures. Nat. Commun. 6, 7579. https://doi.org/10.1038/ncomms8579.
Todd, C., Stone, J.O.H., Conway, H., Hall, B., Bromley, G., 2010. Late quaternary evolution of reedy glacier, Antarctica. Quat. Sci. Rev. 29, 1328–1341.
Westoby, M.J., Dunning, S.A., Woodward, J., Hein, A.S., Marrero, S.M., Winter, K., Sugden, D.E., 2016. Interannual surface evolution of an Antarctic blue-ice moraine using multi-temporal DEMs. Earth Surf. Dyn. 4, 515–529.
Whillans, I.M., Cassidy, W.A., 1983. Catch a falling star: meteorites and old ice. Science 222, 55–57. https://doi.org/10.1126/science.222.4619.55.
Whitehouse, P.L., Bentley, M.J., Le Brocq, A.M., 2012. A deglacial model for Antarctica: geological constraints and glaciological modelling as a basis for a new model of Antarctic glacial isostatic adjustment. Quat. Sci. Rev. 32, 1–24.
Woodward, J., Hein, A., Winter, K., Westoby, M., Marrero, S., Dunning, S., Lim, M., Rivera, A., Sugden, D., 2022. Blue-ice moraines formation in the Heritage Range, West Antarctica: implications for ice sheet history and climate reconstruction. Quaternary Science Advances 6, 100051.